Article

Discovery Medicine 2025; 37(198): 1274–1296
https://doi.org/10.24976/Discov.Med.202537198.112

Construction of a Prognostic Model for Sepsis-Induced Acute Lung Injury Based on Neutrophil Extracellular Traps and Key Inflammatory Genes

Wenxing Zhang[1], Wen Tang[2], Zhao Li[1], Juncai Lu[1], Zhengyu Li[1], Jichao Peng[3], Xiaoran Liu[1,4,5,*]

[1]Emergency and Trauma College, Hainan Medical University, 571199 Haikou, Hainan, China
[2]Department of Orthopedics Center, The First Affiliated Hospital, Hengyang Medical School, University of South China, 421001 Hengyang, Hunan, China
[3]School of Public Health, Hainan Medical University, 571199 Haikou, Hainan, China
[4]Emergency Department, The First Affiliated Hospital of Hainan Medical College, 570102 Haikou, Hainan, China
[5]Key Laboratory of Emergency and Trauma of Ministry of Education, Hainan Medical University, 571199 Haikou, Hainan, China
*Correspondence: hy0203049@muhn.edu.cn (Xiaoran Liu)
Published: 20 July 2025

Background: Sepsis, a life-threatening condition resulting from a dysregulated host response to infection, frequently progresses to acute lung injury (ALI), a severe complication associated with high mortality due to the lack of reliable early-stage biomarkers. Neutrophil extracellular traps (NETs) and the associated inflammatory cascade aggravate disease progression via positive feedback mechanisms. This study aimed to investigate the heterogeneity of NETs- and inflammation-related genes (NIRGs) in sepsis-induced ALI (siALI), construct a diagnostic model, and characterize the immune microenvironment (IME) and its association with immune cell infiltration (ICI).

Methods: Publicly available transcriptomic datasets from the Gene Expression Omnibus (GEO) (GSE66890, GSE32707, GSE10474), GeneCards and relevant literature were used to identify differentially expressed Neutrophil extracellular traps and Inflammatory-Related Differentially Expressed Genes (NIRDEGs), which were subsequently validated. Perturbed biological processes and immune-cell dynamics were examined via Gene Ontology (GO), Kyoto Encyclopedia of Genes and Genomes (KEGG), and Gene Set Enrichment Analysis (GSEA), as well as immune cell deconvolution using CIBERSORT. Multiple machine learning algorithms were employed to construct a diagnosis model, which was evaluated using receiver operating characteristic (ROC) curve analysis, calibration plots, decision curve analysis (DCA), and external validation. Regulatory networks (mRNA-transcription factor, mRNA-miRNA, and mRNA-drug) were constructed using ChIPBase, StarBase 3.0, and the Comparative Toxicogenomics Database (CTD).

Results: Eight genes, S100 Calcium Binding Protein A12 (*S100A12*), Proteinase 3 (*PRTN3*), Toll-like receptor 2 (*TLR2*), triggering receptors expressed on myeloid cells-1 (*TREM1*), Serum and glucocorticoid-induced kinanse-1 (*SGK1*), Phosphatidylinositol-4,5-bisphosphate 3-kinase catalytic subunit gamma (*PIK3CG*), Fibrinogen-like protein 2 (*FGL2*), and Toll-like receptor 8 (*TLR8*), were identified as candidate diagnostic biomarkers and therapeutic targets for siALI. High-risk patients showed enrichment in thrombopoietin (TPO), receptor for advanced glycation end-products (RAGE), Toll-like receptor (TLR), and NOD-like receptor (NLR) signaling pathways. Distinct patterns of ICI effectively distinguished sepsis from siALI, and the identified genes were related to immune regulation.

Conclusions: This study elucidates the molecular architecture and immune microenvironment of siALI, offering a robust foundation for early diagnosis and personalized therapeutic strategies.

Keywords: siALI; NETs; inflammation; diagnostic model; IME

Introduction

Sepsis, a life-threatening syndrome characterized by a dysregulated host response to infection and subsequent multi-organ dysfunction, remains a major global health burden, contributing to high morbidity and mortality rates [1,2]. Approximately 75% of acute lung injury (ALI) cases originate from sepsis. Compared to non-septic ALI, sepsis-induced ALI (siALI) is associated with a more intense inflammatory response, delayed pulmonary recovery, and increased mortality [3,4]. The pathogenesis of siALI is multifaceted, involving alveolar-capillary barrier disruption, dysregulated inflammatory responses, surfactant dysfunction, and coagulopathy, factors that collectively hinder the identification of effective therapeutic targets and reliable biomarkers [5,6]. A surge of pro- and anti-inflammatory

mediators released from diverse cell types drives the pathological progression of siALI [7]. When the equilibrium between these mediators is disrupted, an uncontrolled systemic inflammatory response syndrome (SIRS) may occur, leading to early pulmonary inflammatory edema [8]. In murine models of sepsis, genetic deletion of Z-DNA binding protein (ZBP1), a crucial regulator of pro-inflammatory signaling, was shown to suppress cytokine release, reduce macrophage-endothelial cross-talk, attenuate the inflammatory cascade, and improve endothelial function [9]. Clinically, elevated levels of circulating interleukin-17A (IL-17A) have been associated with worsening organ dysfunction in ALI [10]. Other cytokines, including tumor necrosis factor-α (TNF-α), interleukin-1β (IL-1β), and interleukin-6 (IL-6), have also been proposed as candidate biomarkers for predicting ALI onset and mortality [11].

Neutrophil extracellular traps (NETs) are complex, web-like extracellular structures released by activated neutrophils, consisting of decondensed chromatin, proteins from azurophilic granules such as neutrophil elastase and histones, and modified cytoplasmic proteins [12]. Initially recognized for their role in antimicrobial defense, NETs exert their effects by presenting antimicrobial components that support pathogen clearance and tissue repair within an inflammatory milieu [12]. However, growing evidence implicates NETs in causing direct lung tissue injury, promoting thrombosis, and amplifying inflammatory responses, thereby exacerbating lung injury and disease progression [13]. In patients with acute respiratory distress syndrome (ARDS), the concentration of NETs in bronchoalveolar lavage fluid has been inversely correlated with clinical outcomes [14]. Moreover, animal studies have shown that NETs degradation mitigates pulmonary edema, hemorrhage, and inflammatory cell infiltration [15]. Therefore, identifying genes involved in NETs formation and inflammation may uncover key molecular targets for intervention and diagnosis, thereby facilitating the development of novel therapeutic and diagnostic strategies in siALI.

Bioinformatics, an interdisciplinary field merging biology and computer science, harnesses advanced computational algorithms to analyze complex, high-dimensional biomedical data [16]. Its primary objective is to uncover early disease signatures and elucidate the molecular and cellular mechanisms that drive disease onset and progression. Recent studies have highlighted the predictive value of gene expression profiling for siALI [17]. Gene expression analyses have been central to recent investigations and demonstrate strong potential for diagnosing siALI [18]. For example, one study identified eight signature genes capable of distinguishing healthy individuals from siALI patients [19], while another reported significant upregulation of neutrophil-associated transcripts in affected individuals [20]. Nevertheless, many of these studies were limited by small sample sizes and lacked direct comparative analyses between sepsis and siALI.

In this study, we leveraged Gene Expression Omnibus (GEO) datasets to conduct differential expression analysis (DEA) and employed machine-learning-based bioinformatic pipelines to identify genes associated with both NETs formation and inflammatory pathways in siALI. A diagnostic model was developed, complemented by comprehensive profiling of the immune microenvironment (IME) and assessment of the relationships between NETs- and inflammation-related genes (NIRGs) and immune cell infiltration (ICI). Our findings provide a mechanistic framework that may inform future development of novel targeted therapies and diagnostic tools for siALI.

Materials and Methods

Data Download

In this study, publicly available transcriptomic datasets related to siALI were retrieved from the GEO database [21,22], including GSE66890 [23], GSE32707 [24], and GSE10474 [19]. These datasets encompass diverse clinical sources and detection platforms. All blood or plasma-derived samples were included in the analysis. Detailed dataset characteristics are presented in Table 1.

To systematically identify core genes associated with NETs and inflammation, the GeneCards database [25] was queried using the keywords “NETs” and “Inflammatory”, respectively. Protein-coding genes with relevance scores >1 were selected. These gene lists were further refined and expanded based on published literature [26,27]. After removing duplicates and integrating the data, NETs-related genes (NRGs) and inflammation-related genes (IRGs) were identified [28–30]. The intersection of these two gene sets constituted the final list of NIRGs.

Before data integration, batch effects were corrected using the “sva” R package [31]. The expression matrices of GSE66890 and GSE32707 were subsequently merged to form the GEO training set. The effectiveness of normalization and batch correction was assessed using boxplots and principal component analysis (PCA) [32].

siALI-Associated NIRDEGs

Differential expression analysis (DEA) was conducted in the training set using the “limma” package (version 3.58.1) [33] to identify differentially expressed genes (DEGs) between siALI and sepsis samples. Genes with $|\text{logFC}| > 0$ and $p < 0.05$ were considered differentially expressed. These DEGs were intersected with the predefined NIRG set to obtain the final list of Neutrophil extracellular traps and Inflammatory-Related Differentially Expressed Genes (NIRDEGs). The top 20 most significant NIRDEGs were visualized using a heatmap generated with the “pheatmap” package (version 1.0.12), and their chromosomal distributions were mapped using “RCircos” (version 1.2.2) [34].

Table 1. Summary of dataset characteristics.

Dataset ID	Platform	Species	Sample source	siALI samples	Sepsis samples	Reference (PMID)
GSE66890	GPL6244	*Homo sapiens*	Blood	29	28	25795726
GSE32707	GPL10558	*Homo sapiens*	Whole blood	18	30	22461369
GSE10474	GPL571	*Homo sapiens*	Plasma	13	21	19174476

Abbreviations: siALI, sepsis-induced acute lung Injury.

Validation of Differential Expression and ROC Curve Analysis

To further evaluate the expression differences of NIRDEGs between siALI and sepsis groups in the integrated GEO training dataset, group-wise comparisons were visually depicted based on NIRDEGs expression profiles. The diagnostic performance of individual NIRDEGs for siALI was evaluated using receiver operating characteristic (ROC) curve analysis performed with the "pROC" package (version 1.18.5) in R [35]. The area under the curve (AUC) values were interpreted as follows: 0.5–0.7, marginal; 0.7–0.9, acceptable; and >0.9, exceptional diagnostic accuracy.

GO and KEGG Enrichment Analysis

Gene Ontology (GO) [36] provides functional annotations for genes, while the Kyoto Encyclopedia of Genes and Genomes (KEGG) [37] outlines biological pathways and molecular interactions of genes and genomes. Enrichment analyses of NIRDEGs for GO terms and KEGG pathways were conducted using the "clusterProfiler" package (version 4.10.0) in R [38]. Enrichment results with adjusted p-value (p_{adj}) < 0.05 and false-discovery rate (FDR or q-value) < 0.25 were considered statistically significant. Multiple testing correction was performed using the Benjamini-Hochberg method.

siALI Diagnostic Model Development

A diagnostic mode for siALI was built using the integrated GEO datasets. Logistic regression (LR) was initially applied to the NIRDEGs. Genes meeting the significance threshold ($p < 0.05$) were retained in the final model, and their expression profiles were visualized using a forest plot.

Random forest (RF) analysis was then performed using the "randomForest" package (version 4.7-1.2) [39], incorporating the NIRDEGs identified in the logistic regression model. The model was trained using 1000 decision trees (ntree = 1000). Through five iterations of 10-fold cross-validation, the optimal subset of variables was determined. Genes with a mean decrease in Gini coefficient >1 were selected for subsequent analyses.

Subsequently, support vector machine (SVM) analysis [40] was employed to construct a predictive model based on the NIRDEGs retained from the RF analysis. Gene selection was optimized to balance classification accuracy and error rates, resulting in the identification of NIRDEGs.

Next, Least Absolute Shrinkage and Selection Operator (LASSO) regression analysis was performed using the "glmnet" (version 4.1-8) [41], applied to the NIRDEGs identified by the SVM model. The results were visualized using coefficient path and model plots.

The intersection of genes identified by LR, RF, SVM, and LASSO analyses was designated the final set of model genes. A Venn diagram was generated to illustrate the overlap among the four approaches. A LASSO-derived risk score was calculated based on the corresponding regression coefficients using the following formula:

$$\text{RiskScore} = \sum_i Coefficient\ (gene_i) \times mRNA\ Expression\ (gene_i)$$

Validation of the siALI Diagnostic Model

To evaluate the diagnostic performance of the risk score, the "pROC" package (version 1.18.5) [35] was used to plot the ROC curves and compute AUC values using both the combined GEO dataset and the independent GSE10474 validation set. A nomogram [42] was generated using the "rms" package (version 6.7-1) to visually display the contribution of each model gene to the overall risk of siALI. DCA [43] was conducted using the "ggDCA" package (version 1.1) to evaluate the clinical utility of the diagnostic model by estimating the net benefit across a range of decision thresholds. The thresholds examined ranged from 0 to 1, in increments of 0.01. The analysis was visualized in a decision curve plotted over a threshold range from 0 to 0.6.

Friends Similarity and Correlation Analyses

The functional similarity (Friends) between model genes was quantitatively assessed based on GO annotations [36]. Functional similarity analysis was performed using the "GOSemSim" (version 2.28.0) [44]. To further investigate the relationships among model genes, their expression correlations were examined using Spearman correlation analysis, based on data from the combined GEO dataset. Correlation coefficients were visualized using the "pheatmap" (version 1.0.12) and ggplot2 (version 3.4.4) packages.

Gene Set Enrichment Analysis (GSEA)

To explore the functional enrichment of gene sets in siALI, GSEA [45] was performed. Genes from the integrated GEO dataset were ranked by their logFC values between siALI and sepsis-only samples. GSEA was then performed using "clusterProfiler" (version 4.10.0), with reference gene sets obtained from the MSigDB. Statistical significance was defined as adjusted p-value (p_{adj}) < 0.05 and false discovery rate (FDR or q-value) <0.25.

GSEA Between High- and Low-Risk Groups

Samples in the training cohort were stratified into high-risk and low-risk groups based on the median risk score. DEGs between these groups were identified using the "limma" package (version 3.58.1), ranked by their logFC values. GSEA was performed using "clusterProfiler" (version 4.10.0), with gene sets retrieved from the MSigDB c2.all.v2024.1.Hs.symbols.gmt collection. Pathways significantly enriched in high-risk samples were identified using a significance threshold of $p_{adj} < 0.05$ and FDR (q-value) <0.25.

PPI Network

Protein-Protein Interaction (PPI) networks are powerful tools for systematically investigating complex biological activities within cells, providing insight into intricate biological processes (BPs) and helping clarify numerous biological questions, including signal transduction, gene regulation, and metabolism [46]. Known or predicted PPIs can be explored using the STRING database [47] (https://cn.string-db.org/). A PPI network was constructed based on the model genes, with a minimum interaction score threshold set at >0.150.

To further predict genes functionally related to the hub genes, GeneMANIA [48] (https://genemania.org/), a comprehensive functional gene prediction platform, was employed. This tool integrates PPI, co-expression, and other genomic data to identify genes with functional similarity to the hub genes and to generate a supplementary PPI network.

Regulatory Network Construction

To investigate the regulatory mechanisms underlying model gene expression, transcription factors (TFs) targeting the model genes were identified using "ChIPBase" [49] (http://rna.sysu.edu.cn/chipbase/). Additionally, interactions between miRNAs and model genes were retrieved from StarBase 3.0 [50] (https://starbase.sysu.edu.cn/). For drug-gene interaction prediction, the CTD [51] (https://ctdbase.org/) was used to explore both direct and indirect regulatory associations. All regulatory networks, including mRNA-TF, mRNA-miRNA, and mRNA-drug interactions, were constructed and visualized using "Cytoscape" [52].

Immune Infiltration Analysis

Enrichment scores reflecting relative ICI levels in individual samples were calculated using single-sample GSEA (ssGSEA) [53]. Boxplots were used to illustrate the expression differences of significantly altered immune cells across cohorts in the training set, utilizing the "ggplot2" package (version 3.4.4). The associations between immune cells and model genes were examined via Spearman correlation analysis, with results visualized using the "pheatmap" (version 1.0.12) and "ggplot2" (version 3.4.4) packages in R.

Statistical Analysis

Data integration and statistical analyses were conducted using R (version 4.3.0). For continuous variables, inter-group comparisons were performed using independent Student's t-tests, while comparisons involving three or more cohorts were analyzed via the Kruskal-Wallis test. Correlation coefficients were determined following Spearman correlation analysis. A p-value < 0.05 was considered statistically significant. Significance levels were indicated as follows: $*p < 0.05$, $**p < 0.01$, and $***p < 0.001$.

Results

Technology Roadmap

The overall study design and analytical workflow are presented in Fig. 1.

siALI Dataset Standardization

To assess data comparability, the combined GEO dataset was evaluated using distribution box plots, which showed minimal differences in expression values after batch effect removal (Fig. 2A,B). PCA further confirmed the effectiveness of batch correction, with no obvious clustering biases observed between datasets (Fig. 2C,D). Additionally, expression distribution box plots of the GSE10474 dataset (Fig. 2E,F) showed minimal variation between pre- and post-normalization states.

siALI-Associated NIRDEGs

Differential expression analysis of the training set identified 1620 DEGs, comprising 847 upregulated and 773 downregulated genes, and were visualized using a volcano plot (Fig. 3A). Intersection of the DEGs with the predefined NIRG set resulted in 30 NIRDEGs (Fig. 3B). Expression profiles of the top 20 NIRDEGs were displayed (Fig. 3C). Furthermore, chromosomal mapping of the 30 NIRDEGs was conducted, and a chromosomal location plot was generated (Fig. 3D). Our chromosomal location plot revealed that a majority of the NIRDEGs, including Coagulation Factor III (*F3*), S100 Calcium Binding Protein A12 (*S100A12*), S100 Calcium Binding Protein A8 (*S100A8*), Interferon Gamma Inducible Protein 16 (*IFI16*), Absent In Melanoma 2 (*AIM2*), and Immunoglobulin FcγRIIa receptor (*FCGR2A*), are located on chromosome 1.

Differential Expression Verification and ROC Curve Analysis

A comparative analysis of NIRDEGs expression levels within the training cohort is presented in Fig. 4A, confirming that all 30 NIRDEGs exhibited significant differential expression ($p < 0.05$). ROC curve analysis, performed using the "pROC" package (Fig. 4B–G), demonstrated that 29 NIRDEGs possessed moderate diagnostic potential for distinguishing siALI from sepsis (AUC range: 0.5–0.7), whereas AIM2 achieved superior diagnostic accuracy with an AUC of 0.713.

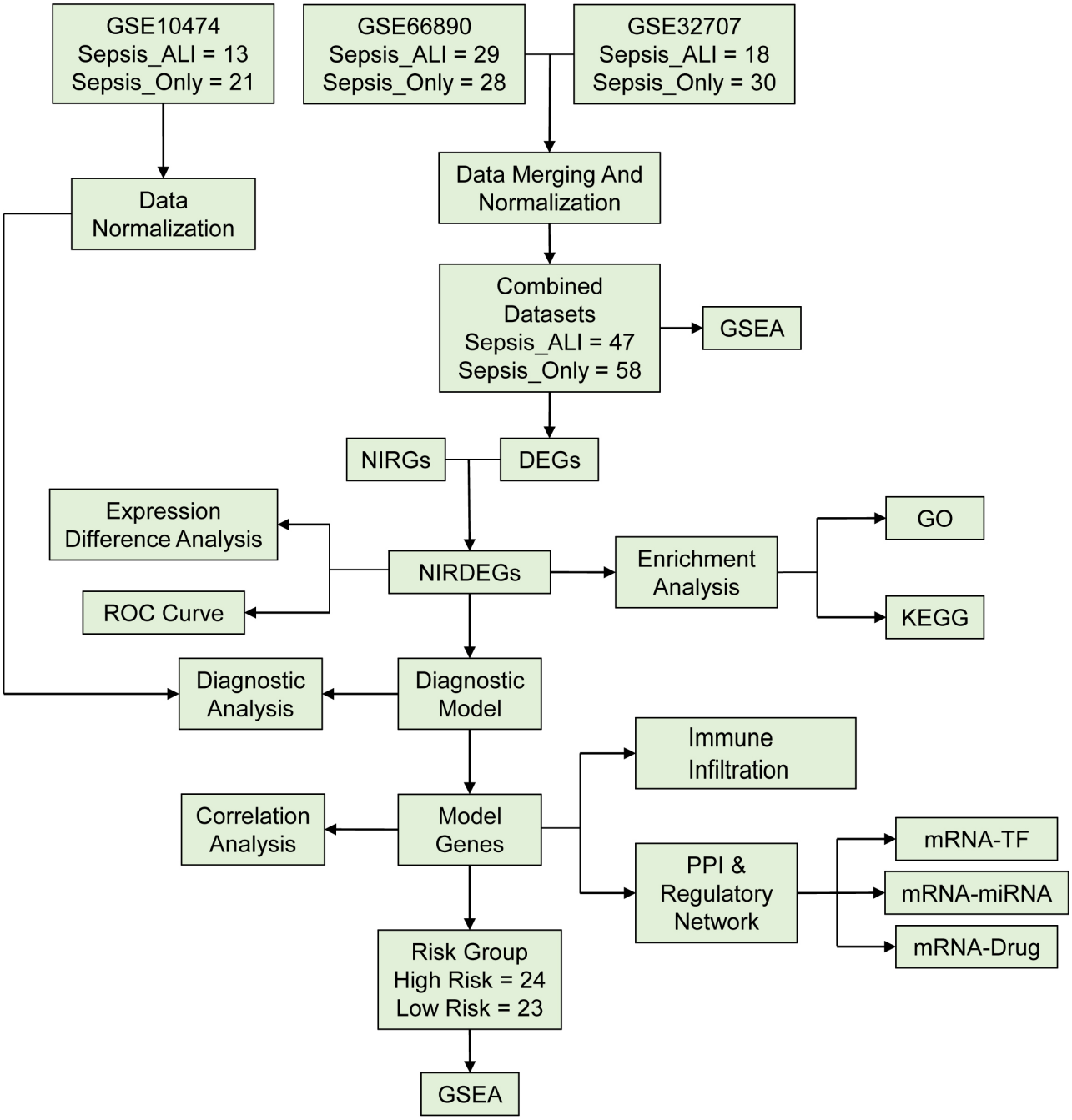

Fig. 1. Flow chart of the comprehensive NIRDEGs analysis. NIRDEGs, NETs- and inflammation-related DEGs; GSEA, Gene Set Enrichment Analysis; NIRGs, NETs- and inflammation-related genes; DEGs, differentially expressed genes; ROC, receiver operating characteristic; GO, Gene Ontology; KEGG, Kyoto Encyclopedia of Genes and Genomes; PPI, Protein-Protein Interaction.

Enrichment Analysis

The results of GO and KEGG were visualized by a bubble chart (Fig. 5A). Gene Ontology enrichment analysis revealed that the 30 NIRDEGs were primarily associated with BPs such as antibacterial defense, cytokine production regulation, foreign cell elimination, and degradation of anatomical structures from external organisms (Fig. 5B). These findings suggest that the identified genes possibly play pivotal roles in inflammatory and immune-related pathways. For cellular component (CC) terms, NIRDEGs were enriched in the secretory granule, cytoplasmic vesicle, vesicle, azurophil granule lumen, and primary lysosome, indicating their potential role in NETs formation (Fig. 5C). Regarding molecular functions (MF), the genes were associated with pattern recognition receptor activity, serine-type endopeptidase activity, serine hydrolase activity, and glycosaminoglycan binding, further suggesting a functional contribution to NETs formation and the initiation of inflammatory and immune responses (Fig. 5D). Ad-

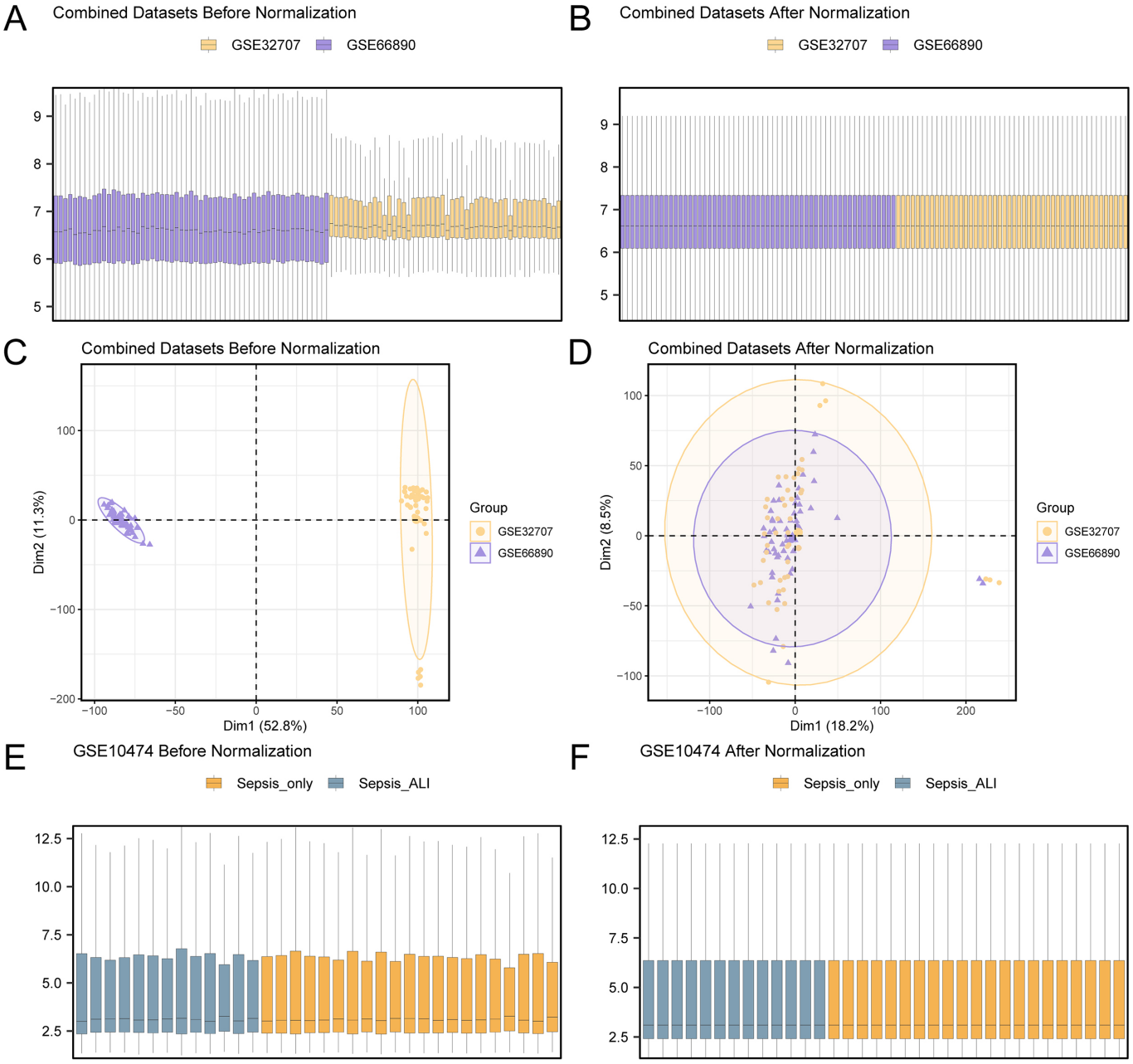

Fig. 2. Removal of batch effects in the siALI datasets. (A) Box plot showing gene expression distribution before batch effect removal. (B) Box plot following batch effect removal. (C) PCA plot before batch effect correction. (D) PCA plot following batch effect correction. (E) Box plot of gene expression distribution in the GSE10474 dataset before normalization. (F) Box plot of gene expression in the GSE10474 dataset following normalization. PCA, principal component analysis.

ditionally, KEGG pathway enrichment analysis identified significant associations with pathways including NETs formation, COVID-19, C-type lectin receptor signaling, Toll-like receptor (TLR) signaling, and tuberculosis, supporting their potential roles in host immunity and inflammation (Fig. 5E).

GSEA for siALI

GSEA identified four significantly enriched pathways in siALI (Fig. 6A). These included several biologically relevant processes and signaling cascades, notably the Kegg Medicus Reference PRNP-PI3K-NOX2 cascade (Fig. 6B), Gilmore's Core NF-κB signaling pathway (Fig. 6C), Reactome's Interleukin-mediated signaling pathway (Fig. 6D), and the WikiPathways (WP) IL-1 signal transduction mechanism (Fig. 6E).

siALI Diagnostic Model Establishment

Logistic regression (LR) was performed using the 30 NIRDEGs, and a diagnostic LR model was developed. All

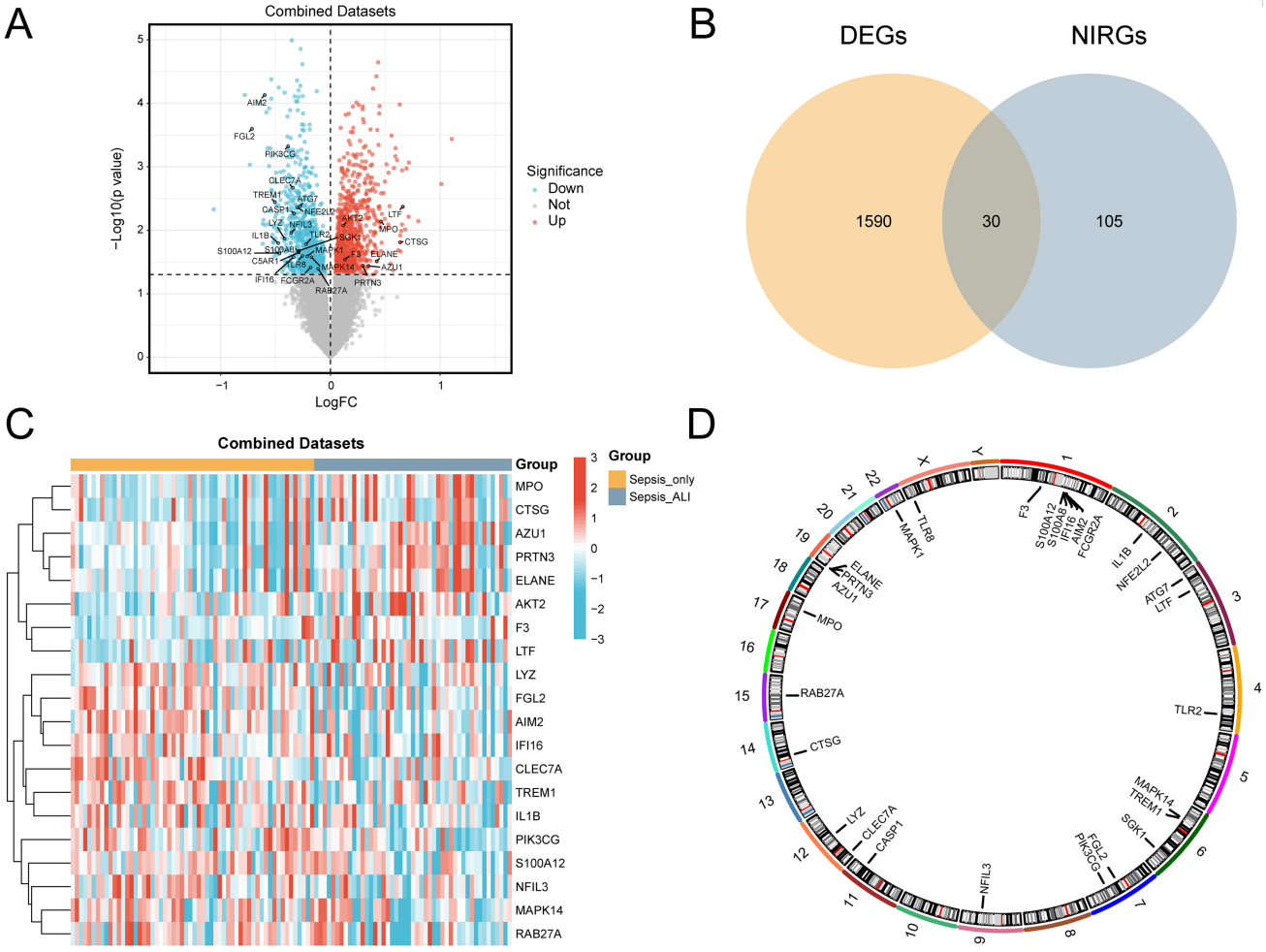

Fig. 3. Differential gene expression analysis and chromosomal distribution of NIRDEGs. (A) Volcano plot showing upregulated and downregulated DEGs. (B) Venn diagram presenting the overlap between DEGs and NIRGs. (C) Heatmap showing NIRDEGs across samples in the integrated GEO dataset. (D) Chromosomal distribution of NIRDEGs. In the heatmap, grey reflects siALI patients, and orange denotes sepsis-only patients. Red indicates high expression, and blue indicates low expression.

30 NIRDEGs were statistically significant ($p < 0.05$), with results presented in a forest plot (Fig. 7A).

Following the initial analysis, the expression profiles of 30 NIRDEGs were analyzed using a random forest (RF) approach to compare the siALI cohort with the sepsis-only controls. The RF model employed 1000 decision trees and a fixed random seed (2024). Model performance assessment revealed stabilization of the error rate at the predetermined tree count (Fig. 7B). To determine key diagnostic markers, MeanDecreaseGini scores were computed for all candidate genes (Fig. 7C), resulting in 28 genes with substantial diagnostic relevance for sepsis-induced lung injury. They included: Lactotransferrin (*LTF*), Myeloperoxidase (*MPO*), AKT serine/threonine kinase 2 (*AKT2*), Cathepsin G (*CTSG*), *F3*, neutrophil elastase (*ELANE*), Proteinase 3 (*PRTN3*), Azurocidin 1 (*AZU1*), *AIM2*, Fibrinogen-like protein 2 (*FGL2*), Phosphatidylinositol-4,5- bisphosphate 3-kinase catalytic subunit gamma (*PIK3CG*), C-Type Lectin Domain Containing 7A (*CLEC7A*), triggering receptors expressed on myeloid cells-1 (*TREM1*), Autophagy Related 7 (*ATG7*), Nuclear Factor Erythroid 2-Related Factor 2 (*NFE2L2*), Caspase-1 (*CASP1*), nuclear factor interleukin 3-regulated (*NFIL3*), Lysozyme (*LYZ*), Interleukin 1 Beta (IL1β), Toll-like receptor 2 (*TLR2*), Serum and glucocorticoid-induced kinanse-1 (*SGK1*), Complement C5a Receptor 1 (*C5AR1*), *S100A12*, Toll-like receptor 8 (*TLR8*), Mitogen-Activated Protein Kinase 1 (*MAPK1*), IFI16, Mitogen-Activated Protein Kinase 14 (*MAPK14*), and Ras-related protein Rab27A (*RAB27A*).

The 28 candidate biomarkers were then incorporated into a support vector machine (SVM)-based predictive framework. Optimization through error minimization (Fig. 7D) and accuracy maximization (Fig. 7E) led to the identification of nine optimal predictive genes: *S100A12*, *PRTN3*, *TLR2*, *TREM1*, *SGK1*, *PIK3CG*, *FGL2*, *TLR8*, and *AZU1*. These nine genes were further subjected to LASSO regression analysis to construct a refined diagnostic model. Model characteristics were illustrated using coeffi-

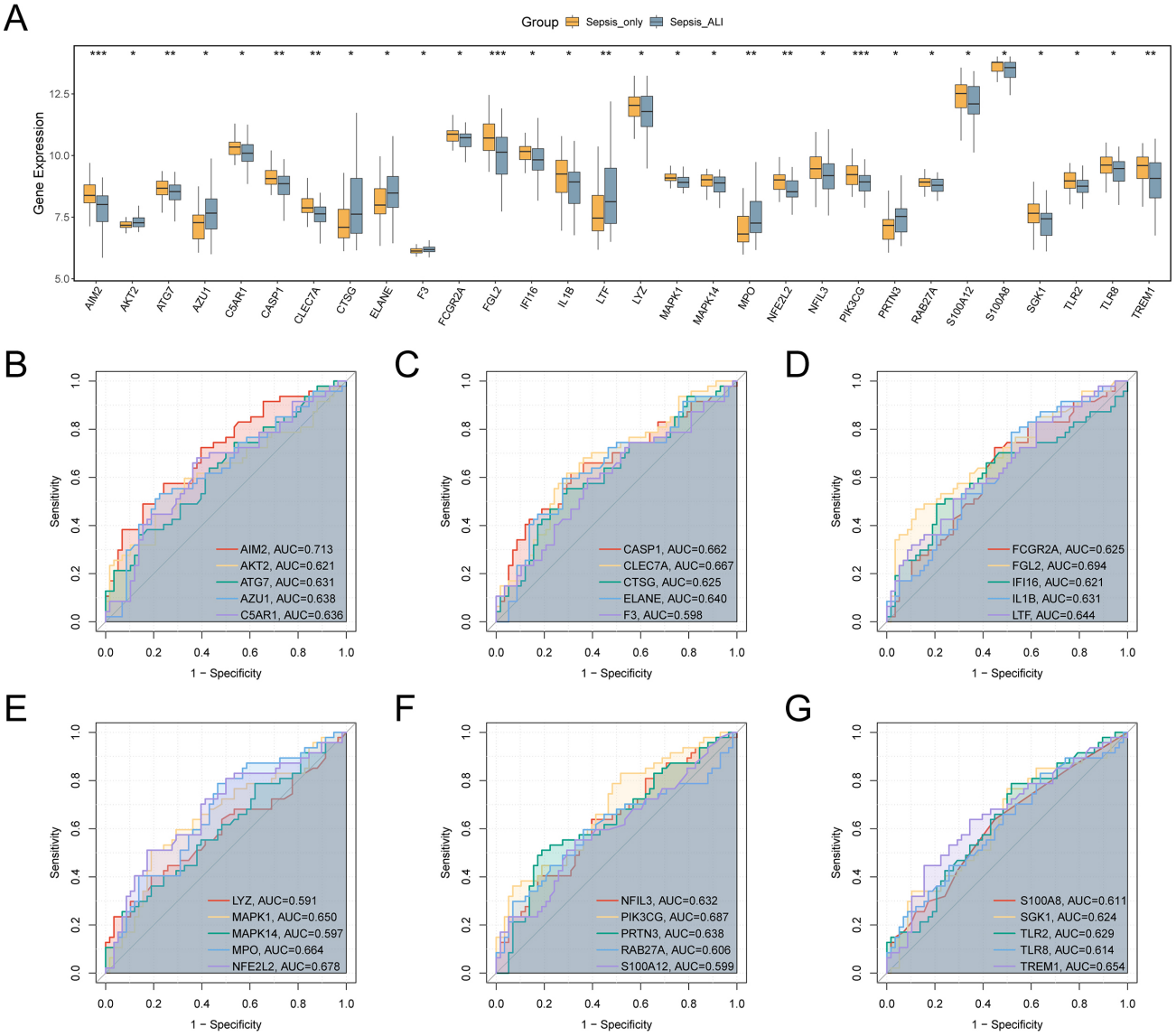

Fig. 4. Validation of NIRDEGs and diagnostic performance. (A) Group comparison plot of NIRDEG expression levels between siALI and sepsis-only samples in the integrated GEO dataset. *$p < 0.05$, **$p < 0.01$, and ***$p < 0.001$. (B–G) ROC curves of selected NIRDEGs based on the training dataset. In the group comparison plot, orange indicates the sepsis-only cohort, and grey indicates the siALI cohort.

cient plots (Fig. 7F) and variable trace diagrams (Fig. 7G). A Venn diagram illustrating gene overlaps among the LR, RF, SVM, and LASSO models is shown in Fig. 7H. This integrative approach yielded eight core diagnostic genes: *S100A12*, *PRTN3*, *TLR2*, *TREM1*, *SGK1*, *PIK3CG*, *FGL2*, and *TLR8*. The final diagnostic model incorporated a LASSO-derived risk assessment metric (RiskScore), computed as follows:

RiskScore = *FGL2* × (–0.607) + *PIK3CG* × (–1.285) + *S100A12* × (–0.517) + *TLR8* × (0.045) + *TREM1* × (–0.533) + *SGK1* × (–0.115) + *TLR2* × (–0.451) + *PRTN3* × (0.589)

Internal Validation and Functional Similarity (Friends) Analysis of the Diagnostic Model for siALI

Internal validation of the model using ROC curve based on the risk score demonstrated strong discriminative power in the training set, with an AUC of 0.843, indicating high diagnostic accuracy (Fig. 8A). The clinical applicability of the siALI model was assessed through a nomogram incorporating the identified biomarker genes (Fig. 8B). Calibration plots demonstrated excellent concordance between predicted and observed outcomes, indicating robust predictive accuracy (Fig. 8C). DCA confirmed the superior net clinical benefit of the model compared to extreme treatment strategies, as indicated by its elevated position on the benefit curve (Fig. 8D).

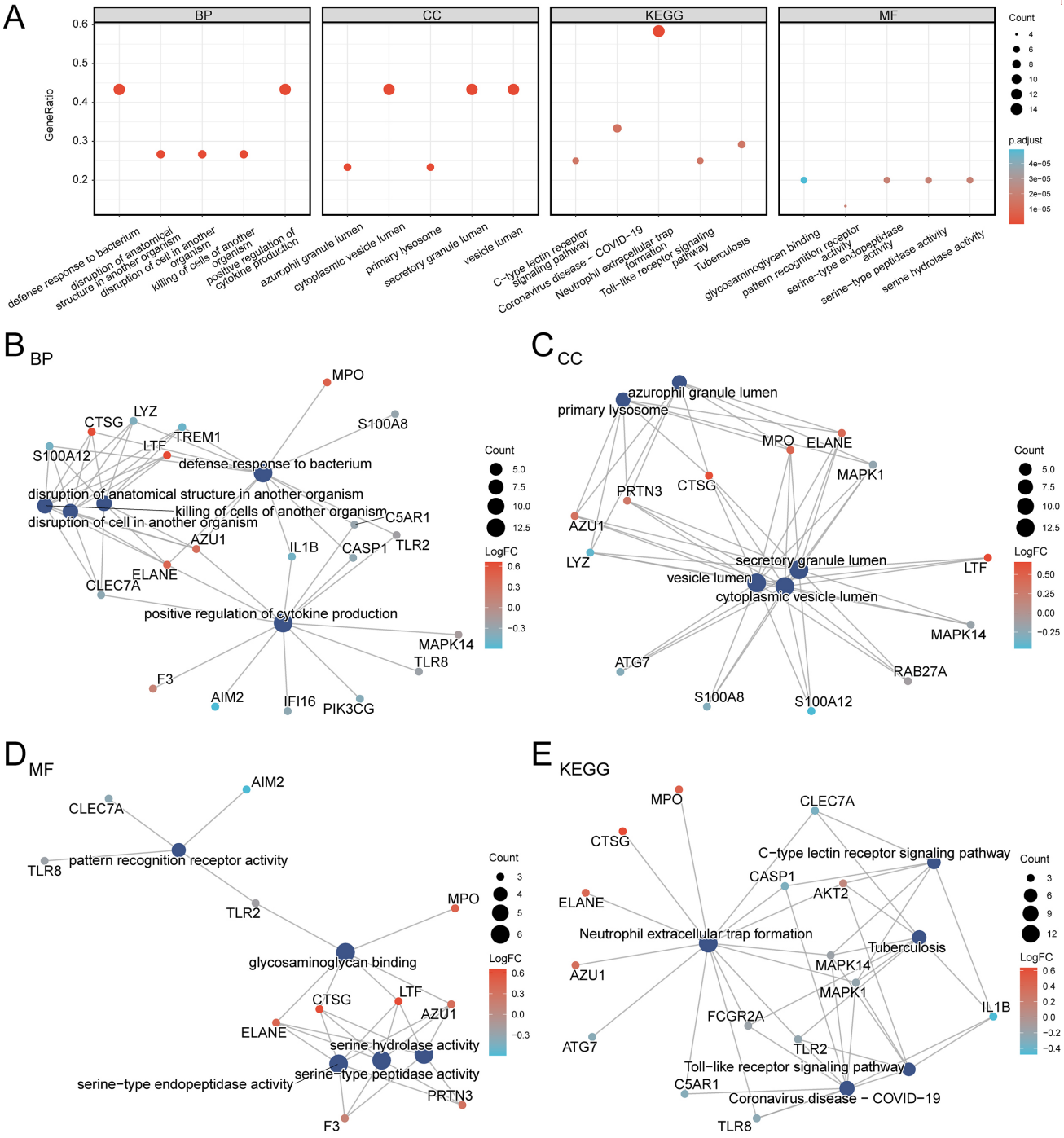

Fig. 5. GO and KEGG enrichment analyses of NIRDEGs. (A) Bubble plot illustrating the results of GO and KEGG pathway enrichment analysis. (B–E) Network diagrams of enrichment results: BPs (B), CCs (C), MFs (D), and KEGG pathways (E). BP, biological processe; CC, cellular component; MF, molecular functions.

Finally, Friends analysis prioritized the candidate genes based on their association with sepsis-induced lung injury pathways (Fig. 8E). Among these, *S100A12* emerged as a potentially key mediator in siALI pathogenesis.

External Validation and Functional Similarity (Friends) Analysis of the Diagnostic Model for siALI

The risk score demonstrated moderate discriminatory ability in the validation dataset (GSE10474), with an AUC of 0.674 (Fig. 9A). Additionally, a nomogram based on the model genes showed that these genes still had diagnostic value in the validation set (Fig. 9B). Calibration analysis was carried out to further assess the model's prediction per-

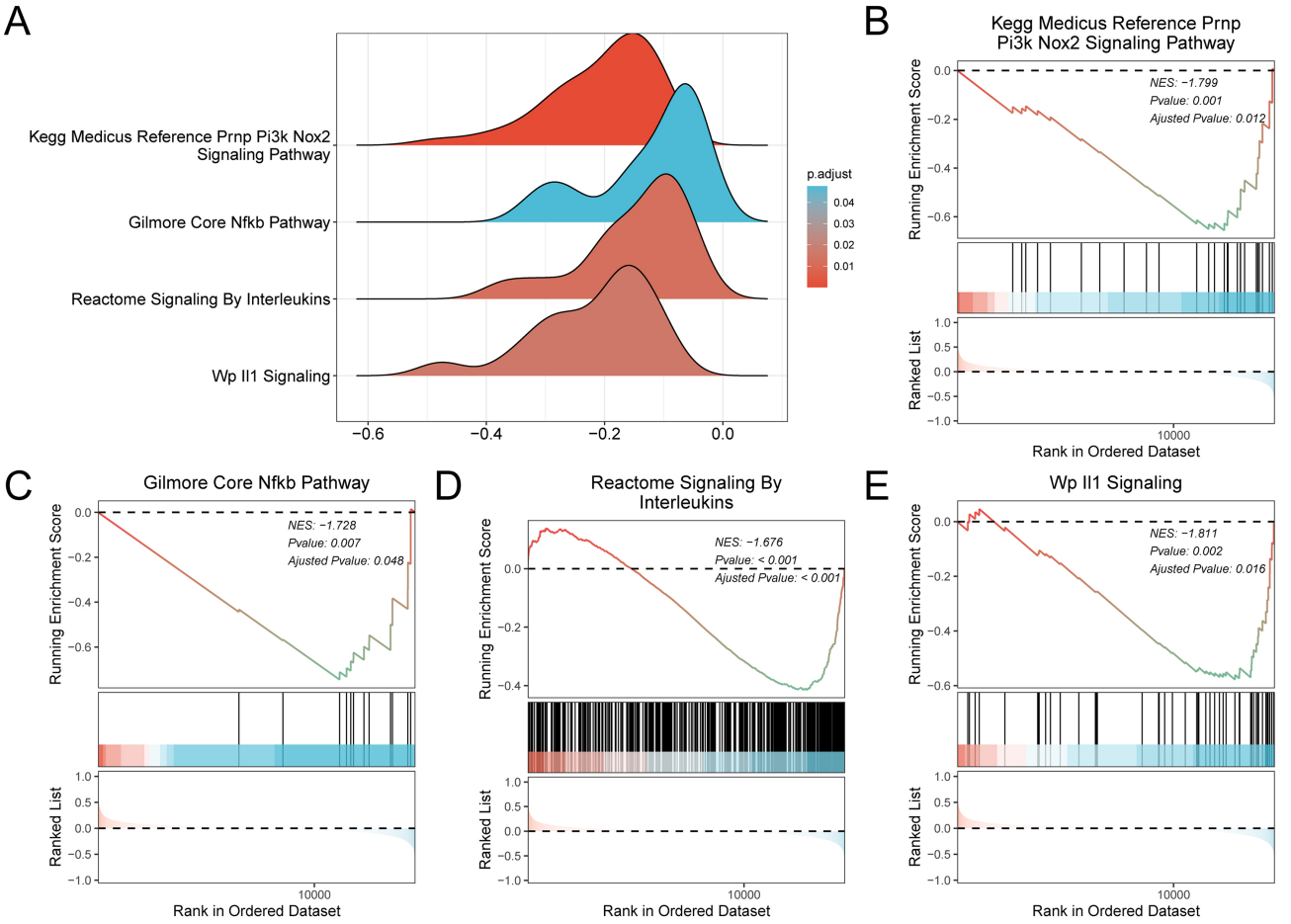

Fig. 6. GSEA of the combined datasets. (A) Ridge plots showing four significantly enriched biological functions identified via GSEA. (B–E) GSEA revealed marked enrichment of DEGs in the KEGG Medicus Reference PRNP-PI3K-NOX2 signaling pathway (B), the Gilmore Core NF-κB pathway (C), the Reactome Signaling by Interleukins pathway (D), and the WP IL-1 signaling pathway (E). WP, WikiPathways.

formance in the validation dataset, and the corresponding calibration curve was plotted (Fig. 9C). Although the calibration curve (dashed line) deviated from the ideal diagonal line, the model still exhibited acceptable predictive ability. DCA in the validation cohort further confirmed the superior net clinical benefit of our model compared to extreme treatment strategies, as evidenced by its elevated position on the benefit curve (Fig. 9D).

Finally, Friends analysis identified key genes involved in siALI by evaluating similarity scores (Fig. 9E). The results highlighted *S100A12* as a key gene in the disease mechanism.

Correlation Analysis of Model Genes

The differential expression of the eight model genes between the high-risk and low-risk groups was illustrated using a group comparison plot (Fig. 10A). Among them, *PIK3CG* and *TLR8* exhibited highly significant expression differences between the risk groups in siALI samples ($p < 0.001$), while *FGL2* and *PRTN3* showed markedly significant differences ($p < 0.01$).

A heatmap displayed the pairwise correlations among the eight model genes (Fig. 10B). Notably, a significant positive relation was observed between *TLR8* and *TLR2* (r = 0.57, $p < 0.05$) (Fig. 10C).

GSEA Between High- and Low-Risk Cohorts

Comparative analysis between the high-risk and low-risk cohorts identified 495 DEGs, including 213 upregulated and 282 downregulated genes (Fig. 11A). The expression profiles of the top 20 DEGs, ranked by their absolute log fold change (|logFC|), were visualized using the "pheatmap" package (Fig. 11B). GSEA revealed four significantly enriched pathways (Fig. 11C), indicating that these DEGs are primarily involved in key biological processes and signaling pathways. These included thrombopoietin (TPO)-mediated signaling (Fig. 11D), receptor-mediated pathways for advanced glycation end-products (Fig. 11E), TLR cascades (Fig. 11F), and NLR signaling mechanisms (Fig. 11G).

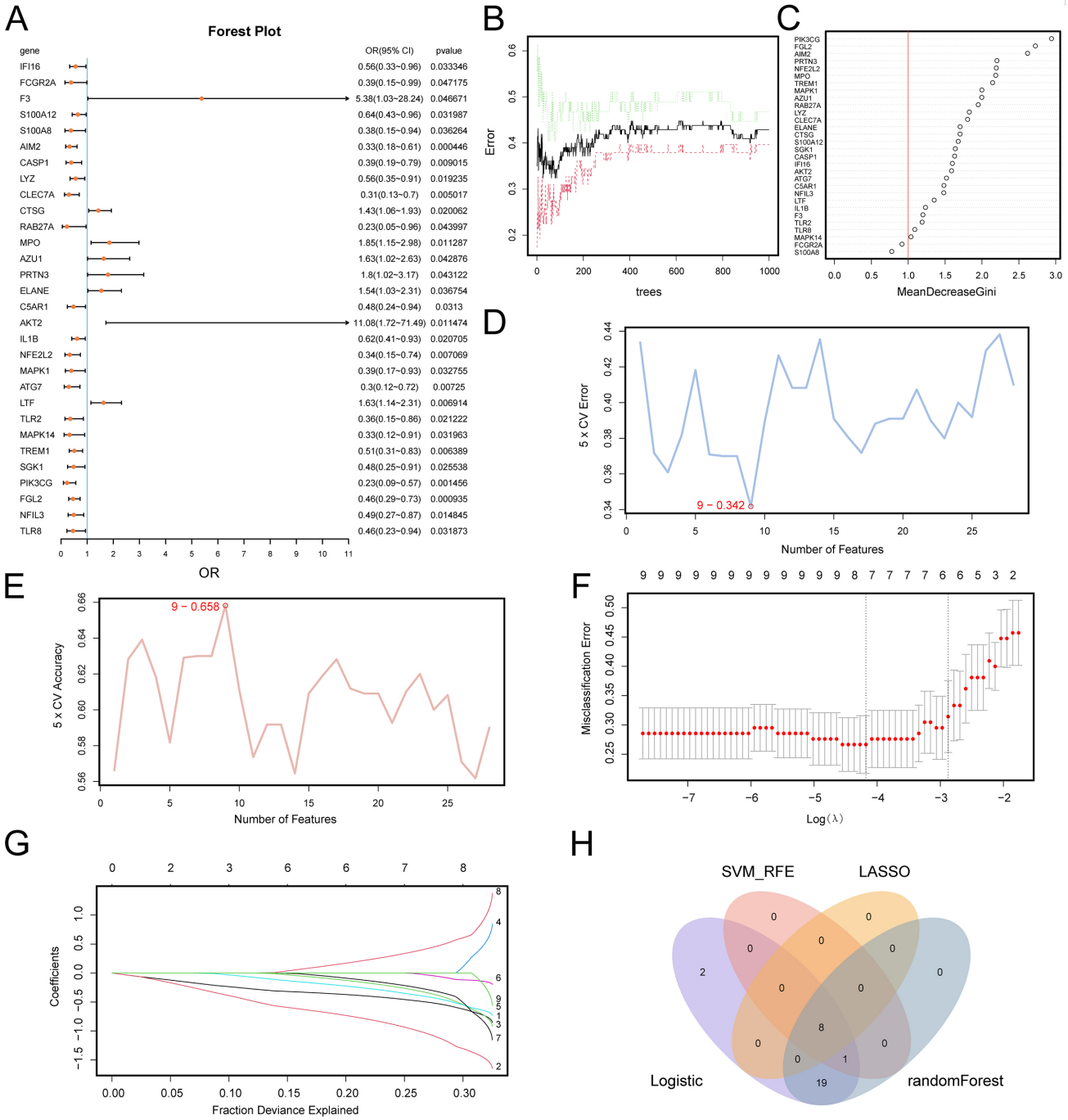

Fig. 7. Construction of the diagnostic model for siALI. (A) Forest plot of the 30 NIRDEGs included in the LR model. (B) Error curve plot of the RF algorithm during training. (C) Scatter plot showing MeanDecreaseGini values for NIRDEGs, arranged in descending order. (D,E) Plots showing the number of genes yielding the lowest classification error (D) and highest accuracy (E) in the SVM model. (F,G) LASSO regression model plot (F) and variable trace plot (G). (H) Venn diagram showing the overlapping genes identified by LR, RF, SVM, and LASSO analyses. SVM, support vector machine; LR, Logistic regression; RF, Random forest; LASSO, Least Absolute Shrinkage and Selection Operator.

PPI Network

A PPI network comprising the eight model genes was constructed using the STRING database (Fig. 12A). Additionally, a broader interaction network including the eight model genes and their functionally related counterparts was generated through the GeneMANIA platform (Fig. 12B). This expanded network comprised a total of 28 genes, encompassing the original eight model genes and 20 functionally associated proteins.

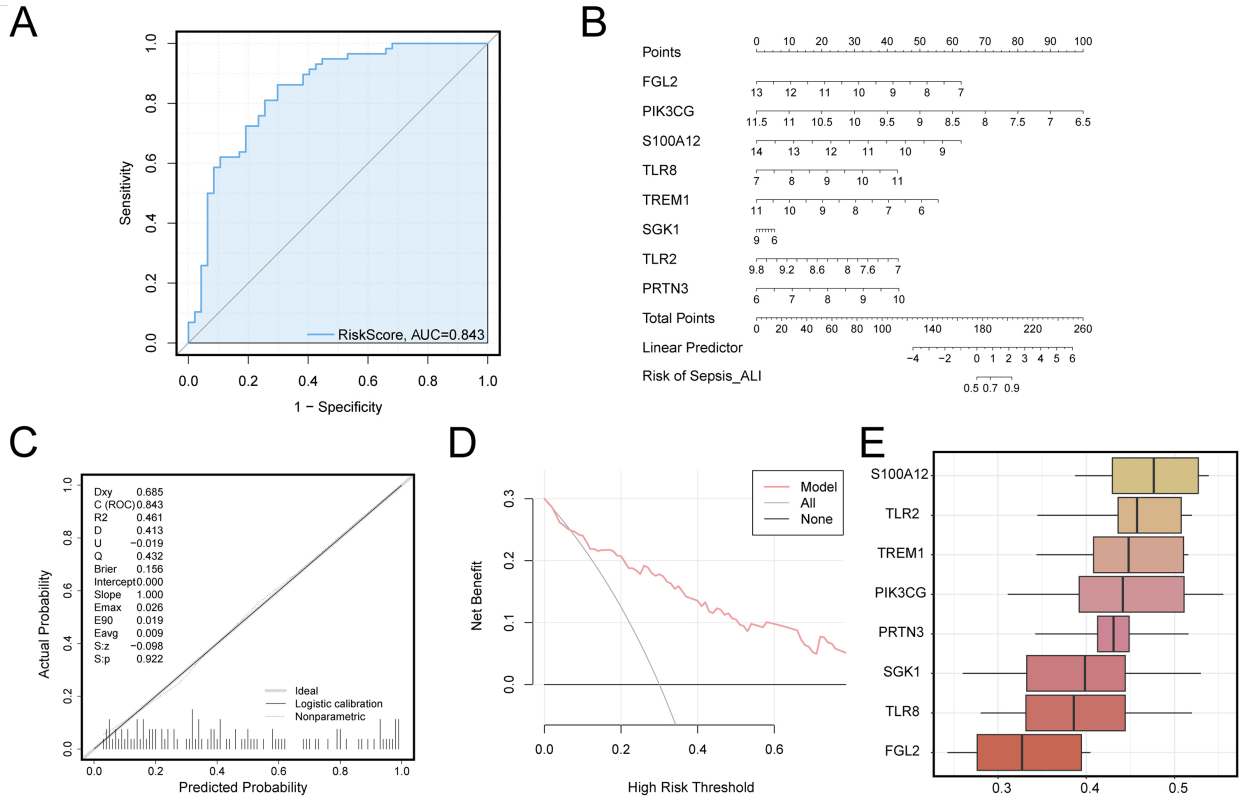

Fig. 8. Internal validation and Friends analysis of the diagnostic model. (A) ROC curve of the risk score based on the integrated GEO dataset. (B) Nomogram constructed from the identified model genes. (C,D) Calibration curve (C) and DCA (D) of the risk score. In the DCA plot, the y-axis represents net benefit, and the x-axis shows threshold probability. (E) Box plot showing the Friends analysis results for the model genes. DCA, decision curve analysis.

Regulatory Network Construction

The mRNA-transcription factor (TF) regulatory network comprised five model genes and 46 TFs (Fig. 13A). An mRNA-miRNA regulatory network was also constructed, comprising one model gene and 35 microRNAs (Fig. 13B). Additionally, an mRNA-drug regulatory network was established, involving seven model genes and 31 drugs or molecular compounds (Fig. 13C).

Immune Infiltration Analysis

The ssGSEA method was applied to the training dataset to estimate enrichment scores and evaluate interactions among 28 immune cell populations. Immune cell types showing statistically significant differences ($p < 0.05$) between the siALI and sepsis-only groups were identified and visualized using comparative group plots. As shown in Fig. 14A, seven immune cell types displayed statistically significant differences in infiltration: activated B cells and neutrophils showed significant differences ($p < 0.05$); macrophages and natural killer (NK) T cells showed highly significant differences ($p < 0.01$); eosinophils, myeloid-derived suppressor cells (MDSCs), and T follicular helper (Tfh) cells exhibited significant differences ($p < 0.001$).

Subsequently, the interactions among the seven differentially infiltrated immune cell types within the integrated GEO dataset were visualized using a correlation heatmap (Fig. 14B). The analysis revealed predominantly positive associations among most immune cell populations. Notably, MDSCs and Tfh cells demonstrated a moderate positive correlation ($r = 0.603$, $p < 0.05$), while eosinophils and neutrophils also exhibited a marked positive relation ($r = 0.517$, $p < 0.05$).

Moreover, correlations between the eight model genes and the seven differentially infiltrated immune cell types were examined and presented using a correlation heatmap and a bubble plot (Fig. 14C). Key findings included a negative correlation between *S100A12* and activated B cells, a positive association of *PRTN3* with macrophages, and a favorable correlation between *TLR2* and neutrophils. *TREM1* and *SGK1* exhibited positive relationships with Tfh cells, eosinophils, macrophages, MDSCs, NK T cells, and neutrophils. *FGL2* showed positive correlations with MDSCs, eosinophils, NK T cells, Tfh cells, and macrophages. *TLR8* was positively correlated with eosinophils and neutrophils, but negatively associated with activated B cells. The strongest correlation was observed between *TLR8* and neutrophils ($r = 0.61$, $p < 0.05$).

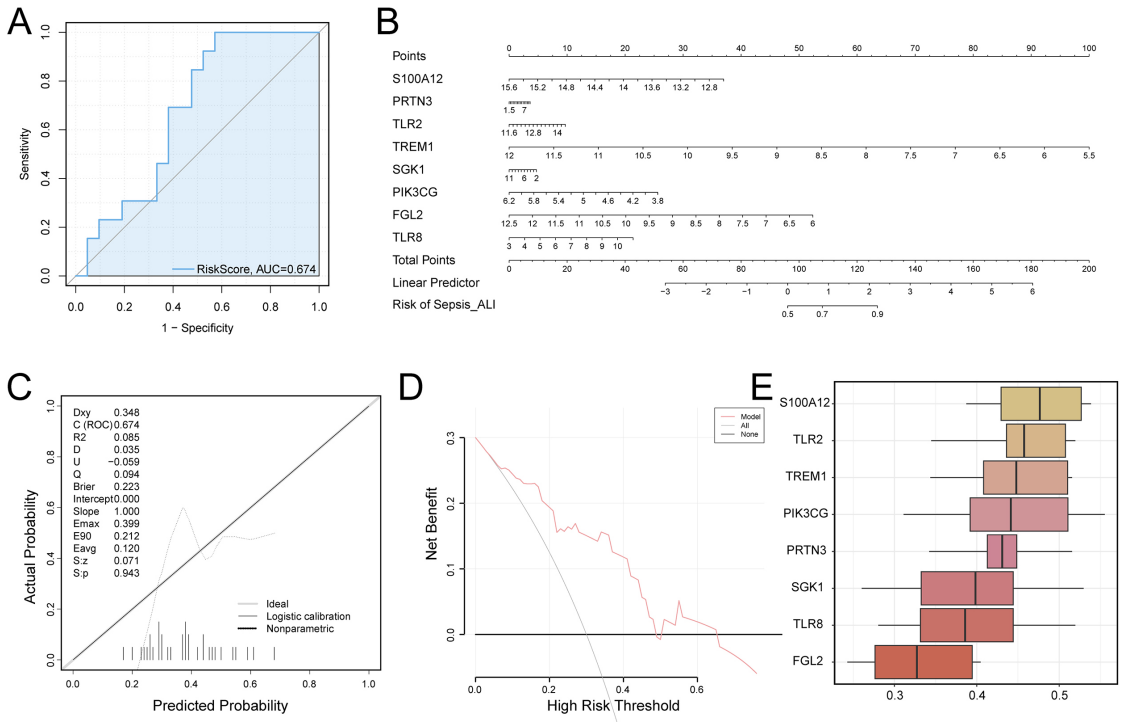

Fig. 9. External validation using GSE10474 and Friends analysis. (A) ROC curve of the risk score in the GSE10474 validation dataset. (B) Nomogram constructed from model genes in the GSE10474 dataset. (C,D) Calibration curve (C) and DCA (D) of the risk score for the diagnostic model in GSE10474. In the DCA plot, the y-axis indicates net clinical benefit, and the x-axis denotes threshold probability. (E) Box plot showing Friends analysis results for the model genes based on the validation dataset.

Discussion

This study systematically identified and validated key genes and molecular pathways associated with NETs and inflammation in siALI via a comprehensive evaluation framework based on bioinformatics. The goal was to elucidate the potential pathological mechanisms by which NETs and inflammatory processes contribute to siALI development and explore their diagnostic potential, thereby presenting novel insights for future research and clinical applications.

A total of 1620 DEGs were identified from blood samples of the siALI and sepsis cohorts. GSEA revealed that these DEGs were primarily enriched in pathways such as IL-1 signaling, interleukin-mediated signaling cascades, the NF-κB core pathway, and the PI3K/AKT/NOX2 signaling axis. These findings highlight a strong association between the identified DEGs and both NETs formation and inflammatory responses. ROC analysis further confirmed that the NIRDEGs possessed moderate diagnostic value in distinguishing siALI from sepsis. Functionally, these genes play central roles in antibacterial defense, cytokine secretion, and disruption of cellular and tissue integrity in distal anatomical regions. Enrichment analysis indicated significant involvement in key immune-related pathways, including NETs formation, C-type lectin receptor (CLR) signaling, and TLR signaling pathways.

CLRs, primarily expressed on myeloid cells, constitute a diverse family of receptors with multiple subtypes and capable of recognizing diverse ligands. These receptors mediate key immune functions such as phagocytosis, cytokine production, and antigen presentation, playing essential roles in immune surveillance and regulation [54]. In the pulmonary endothelium, upregulated CLRs can stimulate cytokine and chemokine production, ameliorating the innate immune response and mitigating lung injury [55]. Notably, C-type lectin domain family 4, member A (CLEC4A) has been shown to facilitate NETs formation and enhance the release of pro-inflammatory cytokines, thereby intensifying pulmonary inflammation [56]. Similarly, TLRs serve as pattern recognition receptors that initiate innate immune signaling cascades upon pathogen detection [57]. Suppression of the TLR4/Nrf2/NF-κB signaling axis by bacterial protease inhibitors or trypsin inhibitors has been found to alleviate lipopolysaccharide (LPS)-induced ALI [58]. Collectively, these findings further prove the significant role of NIRDEGs in NETs formation, immune defense, and inflammatory processes, implicating them as key contributors to siALI pathogenesis. Consequently, these genes may serve as potential therapeutic targets and diagnostic biomarkers for siALI.

To translate these findings into clinical application, the 30 identified NIRDEGs were subjected to feature selection via LR, RF, SVM, and LASSO regression analyses. This

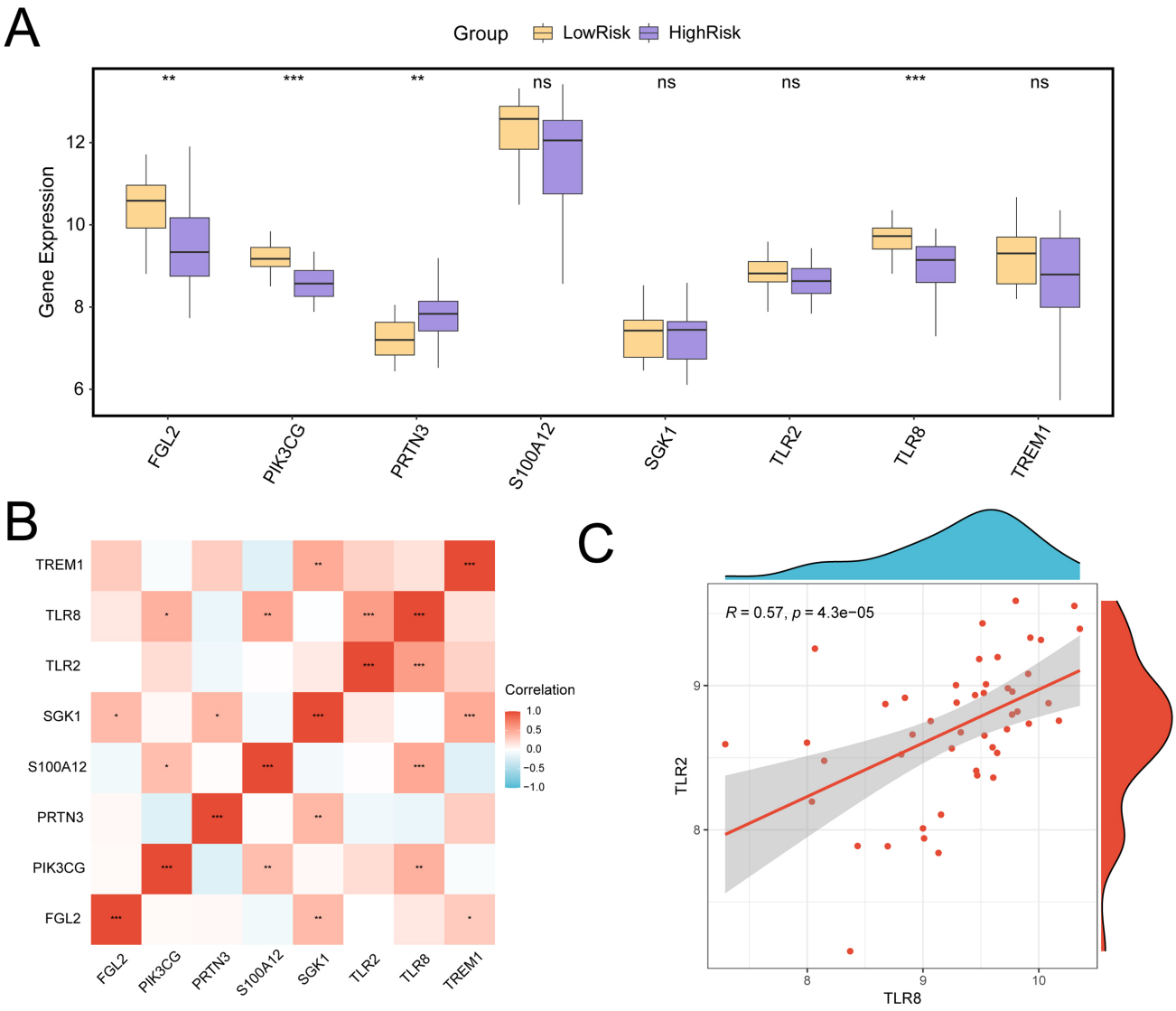

Fig. 10. Correlation analysis of model genes. (A) Group comparison plot of model gene expression between high-risk and low-risk cohorts in siALI samples. (B) Heatmap showing correlations among the model genes. (C) Scatter plot illustrating the correlation between TLR8 and TLR2. Correlation coefficients <0.3 suggest minimal association, 0.3–0.5 denotes a weak correlation, while 0.5–0.8 indicates a moderate association. Positive correlations are shown in red, negative correlations in blue, with color saturation indicating strength. Statistical significance is indicated as $*p < 0.05$, $**p < 0.01$, and $***p < 0.001$. ns, no statistical significance; TLR8, Toll-like receptor 8; *TLR2*, Toll-like receptor 2.

integrative approach led to the identification of eight key biomarker genes: *S100A12*, *PRTN3*, *TLR2*, *TREM1*, *SGK1*, *PIK3CG*, *FGL2*, and *TLR8*.

S100A12, a member of the myeloid-related S100 protein subfamily, plays a pivotal role in host defense against microbial infections and the maintenance of immune homeostasis. It exerts antimicrobial activity by chelating essential metal ions required for pathogen proliferation and interacts with cell surface receptors to activate pro-inflammatory signaling pathways, stimulate cytokine production, and modulate immune responses. Due to its sensitivity to pathological alterations, S100A12 has been proposed as a potential biomarker for disease detection and monitoring [59]. S100A12 and soluble receptors for advanced glycation end-products (sRAGE) are elevated in the serum of siALI patients and mouse models, leading to activation of the NLRP3 inflammasome and increased expression of inflammatory cytokines, adhesion molecules, and apoptosis-related factors. Therefore, S100A12 is a potential biomarker for diagnosing sepsis-induced acute respiratory distress (ARD) [60]. In allergic pneumonia models, S100A12 is highly expressed in neutrophils, and its inhibition has been shown to alleviate airway smooth muscle hypertrophy, reduce inflammation, and suppress airway hyperresponsiveness [61]. Taken together with our findings, these observations suggest that the upregulation

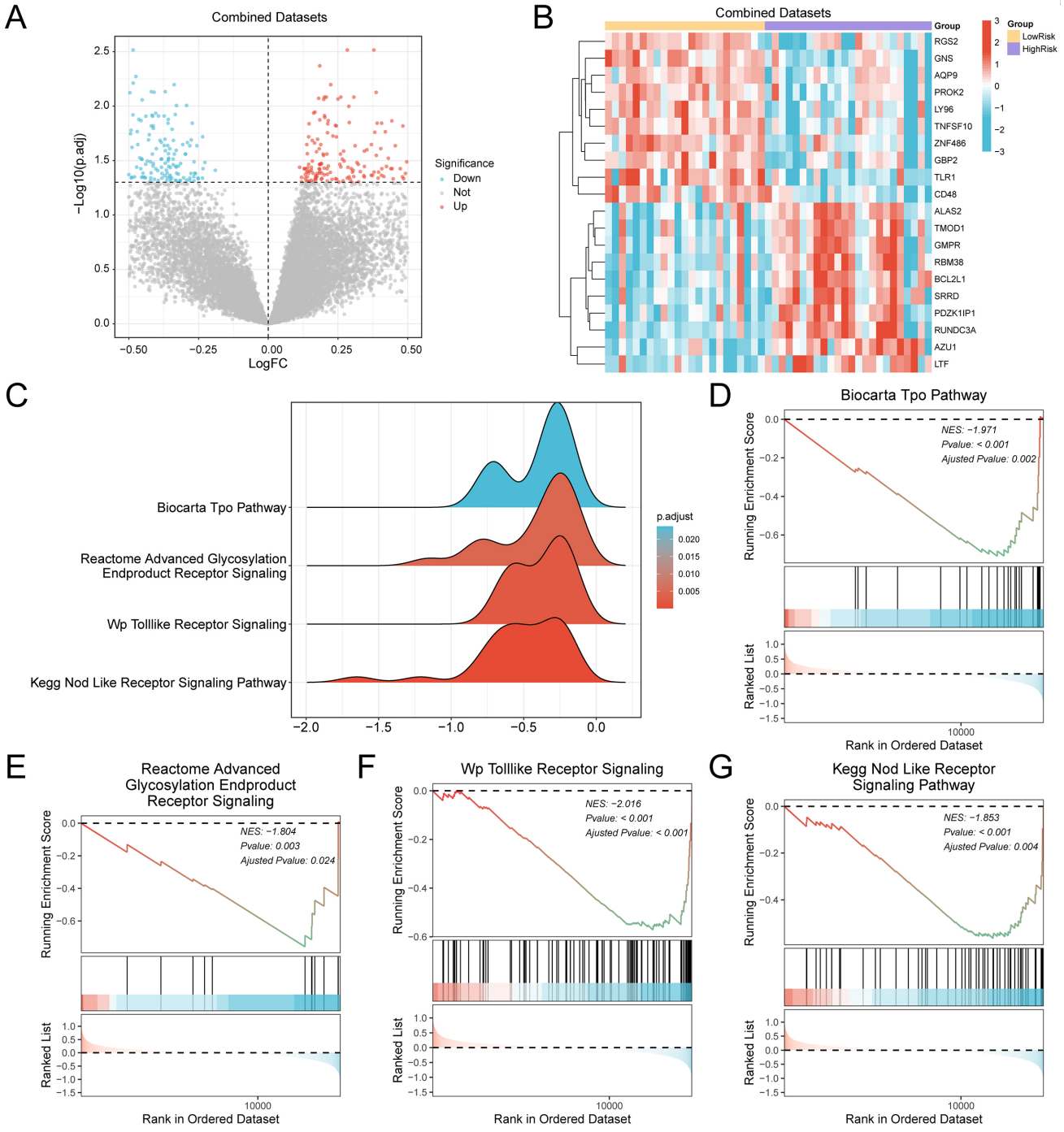

Fig. 11. Differential gene expression analysis and GSEA between high- and low-risk cohorts. (A) Volcano plot of DEGs between high- and low-risk siALI cohorts. (B) Heatmap showing expression of the top 20 DEGs. (C) Ridge plots showing four significantly enriched biological functions identified via GSEA. (D–G) GSEA revealed marked enrichment of DEGs in the Biocarta TPO pathway (D), Reactome Advanced Glycosylation Endproduct Receptor signaling pathway (E), WP TLR signaling pathway (F), and KEGG NLR signaling pathway (G). TPO, thrombopoietin; TLR, Toll-like receptor.

of S100A12 during sepsis contributes to lung injury by amplifying inflammatory responses. Moreover, although S100A12 demonstrates high sensitivity, it has a relatively short biological half-life. Its serum levels rise early following injury in postoperative siALI patients, while bronchoalveolar lavage fluid concentrations gradually decline over time [62]. In our study, Friends analysis further confirmed that S100A12 is central to disease progression, further demonstrating its potential as a novel therapeutic target and diagnostic biomarker for siALI.

PRTN3, a member of the serine protease family, is localized within the azurophilic granules of neutrophils. Fol-

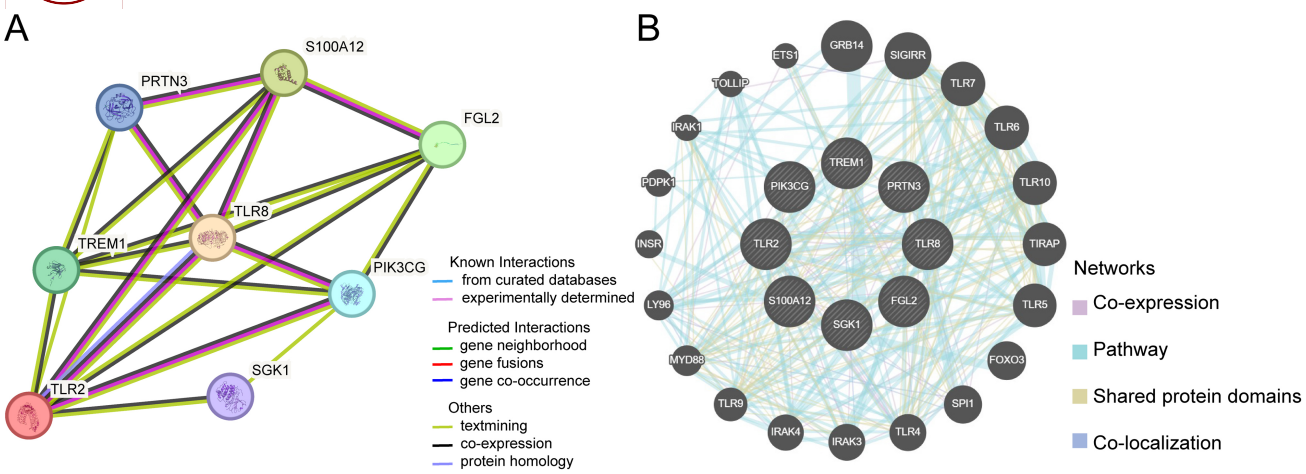

Fig. 12. PPI network analysis of model genes. (A) PPI network of model genes constructed using the STRING database. (B) Interaction network of functionally similar genes predicted by GeneMANIA. Circles represent the model genes and their associated functional partners. Colored lines denote types of functional relationships: The sky blue represents protein interactions from experimental data and literature records; Pink-purple represents experimentally validated PPIs. Green lines represent evidence of gene proximity; Red lines represent evidence of gene fusion; Dark blue lines represent evidence of gene co-occurrence; Yellow-green lines represent evidence of interaction identified through literature mining; Black lines represent evidence of gene co-expression; Blue-purple lines represent evidence of homologous proteins.

lowing neutrophil activation, it is released into the extracellular environment where it contributes to pathogen elimination [63]. Elevated PRTN3 expression has been detected in the blood of COVID-19 patients, with its levels positively correlating with disease severity [64]. However, specific evidence defining the role of PRTN3 in siALI remains limited and requires further investigation.

TLR2, a pattern recognition receptor (PRR) within the innate immune system, is essential for the early recognition of invading microorganisms and endogenous danger signals through its recognition of pathogen-associated molecular patterns (PAMPs) and damage-associated molecular patterns (DAMPs) [65]. In a model of endothelial cell injury, miR-328-3p was shown to target TLR2, thereby suppressing NETs formation [66]. TLR2 also acts as a key upstream receptor in the activation of the ERK1/2 signaling pathway, which mediates autophagy, an essential homeostatic process in mammalian cells involved in immune responses [67]. In murine sepsis models, enhanced autophagy was associated with improved survival outcomes through promotion of NETs formation, whereas autophagy inhibition in traumatic brain injury-induced ALI models aggravated pulmonary pathology [68,69]. However, the precise molecular regulatory network linking autophagy, NETs, and inflammation remains incompletely defined. Based on the present findings, it is hypothesized that downregulation of *TLR2* may contribute to siALI progression by inhibiting autophagy. However, these mechanistic pathways warrant further experimental validation.

Triggering Receptor Expressed on Myeloid cells-1 (TREM-1), expressed on immune cells, acts as a critical regulator of inflammation. Upon activation, it initiates signaling cascades that promote the release of pro-inflammatory mediators, thereby amplifying the inflammatory response [70]. Although upregulation of TREM-1 strengthens immune defense and facilitates pathogen clearance, it can also exacerbate tissue injury and contribute to organ dysfunction [71,72]. Additionally, TREM-1 plays a role in mitochondrial metabolism and energy production [73]. In this study, TREM-1 expression was downregulated in siALI patients, which may impair the NETs formation and compromise pathogen elimination. Furthermore, reduced TREM-1 expression could result in mitochondrial dysfunction, thereby impairing cellular proliferation and tissue repair, ultimately contributing to disease progression.

SGK1, a stress-responsive gene, regulates the differentiation of various immune cells such as T cells, macrophages, and neutrophils, thereby exerting immunomodulatory and anti-inflammatory functions [74]. However, our findings demonstrated that *SGK1* expression was decreased in siALI patients, which may promote lung injury by impairing alveolar fluid clearance [75]. In experimental models investigating the amelioration of sepsis-induced lung injury by melatonin, it has been demonstrated that melatonin mitigates lung damage and enhances survival by increasing alveolar epithelial sodium channel activity. This occurs through activation of the silent information regulator (SIRT1)/SGK1/Neural precursor cell expressed developmentally down-regulated gene 4-like (Nedd4-2) signaling pathway, thereby improving alveolar clearance [75].

Fibrinogen-like protein 2 (FGL2) is a multifunctional immunoregulatory protein that serves as an essential immunosuppressive effector molecule of regulatory T cells

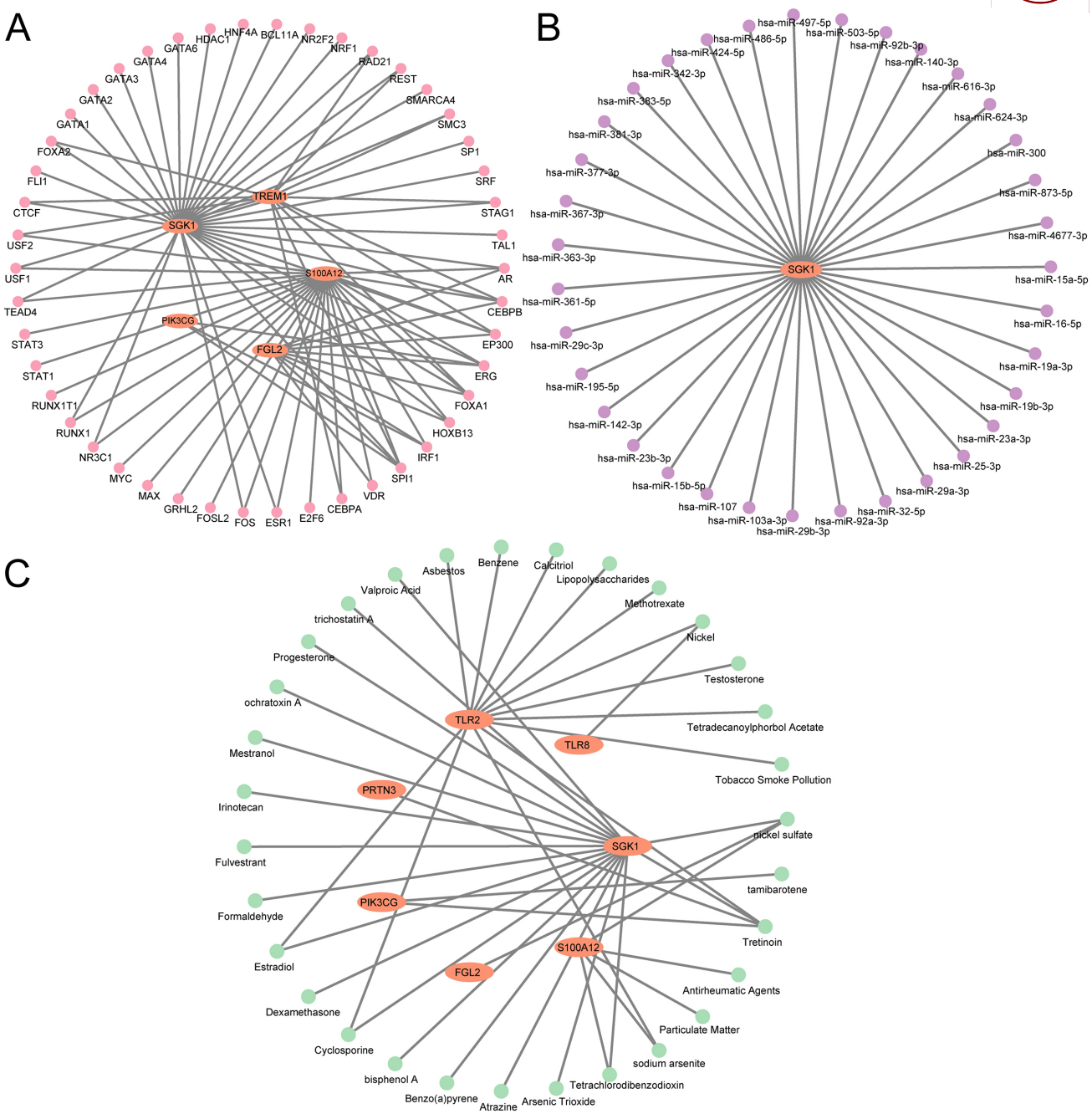

Fig. 13. Regulatory network of model genes. (A) mRNA-TF regulatory network. (B) mRNA-miRNA regulatory network. (C) mRNA-drug interaction network. Node color codes: Orange, mRNAs; Pink, TFs; Purple, miRNAs; Green, drugs or small-molecule compounds.

(Tregs). FGL2 suppresses the expression of Th1 cytokines while simultaneously promoting Th2 cytokine production [76]. Th2 cytokines function as effective anti-inflammatory mediators, reducing inflammatory cell infiltration in lung tissues and mitigating pulmonary inflammation [77]. Moreover, studies suggest that FGL2 promotes neutrophil apoptosis and clearance through interaction with monocytes, thereby accelerating the resolution of sepsis [78]. In murine sepsis models, reduced FGL2 expression has been associated with worsened inflammatory outcomes [79].

TLR8, a member of the pattern recognition receptor family within the innate immune system, is expressed on monocytes, neutrophils, and macrophages, and plays a pivotal role in innate immune regulation [80]. Studies have shown that infants infected with human respiratory syncytial virus exhibit reduced TLR8 levels, while levels increase during the recovery phase [81]. Severe COVID-19 is associated with diminished expression of TLR7 and TLR8. Notably, critically ill patients showed reduced mRNA levels of TLR7 and TLR8 in macrophages and epithelial cells derived from bronchoalveolar lavage fluid [82].

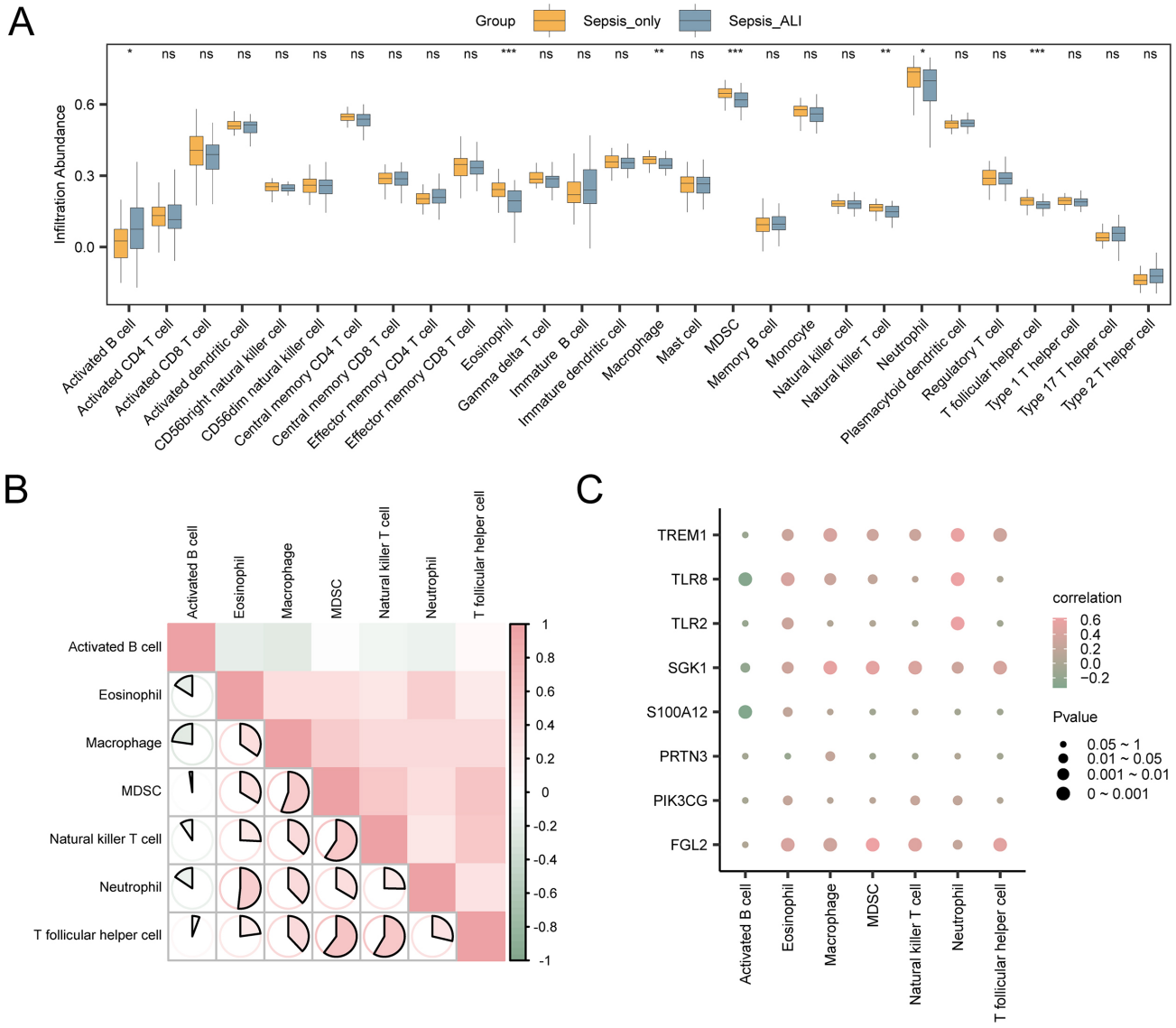

Fig. 14. Immune infiltration analysis using the ssGSEA algorithm. (A) Comparative analysis of ICI profiles between the sepsis-associated ALI (gray) and sepsis-only (orange) groups. $*p < 0.05$, $**p < 0.01$, and $***p < 0.001$. ns, no statistical significance. (B) Heatmap showing correlations among immune cell populations in the integrated GEO dataset. (C) Bubble chart illustrating associations between candidate genes and levels of immune cell infiltration. Correlation strength is categories: negligible ($|r| < 0.3$), weak ($0.3 \leq |r| < 0.5$), moderate ($0.5 \leq |r| < 0.8$), and strong ($|r| \geq 0.8$). Color represents direction of correlation (pink = positive, green = negative) with saturation indicating magnitude. ICI, immune cell infiltration.

Suppression of *PIK3CG* impairs macrophage recruitment and decreases bacterial clearance, thereby promoting the progression of streptococcal pneumonia [83]. This study suggests that reduced expression of *PIK3CG* in siALI may result in diminished NETs formation, leading to impaired bacterial clearance and consequently contributing to the development of lung injury.

Our diagnostic prediction model was constructed based on eight hub genes. Calibration and decision curve analyses demonstrated robust predictive performance across both internal and external datasets in differentiating sepsis from siALI, yielding a high net clinical benefit. The identified hub genes exhibited functional interconnections, suggesting potential synergistic roles in disease pathogenesis. Further stratification of the siALI cohort into high- and low-risk groups revealed significant differential expression of *PIK3CG*, *TLR8*, *FGL2*, and *PRTN3*. Among these, *PIK3CG*, *TLR8*, and *FGL2* were downregulated, while *PRTN3* was upregulated in the high-risk group. GSEA indicated the main enrichment of associated DEGs in TPO, NLR, and TLR pathways, as well as signaling routes involving advanced glycation end-product. These findings highlight key molecular pathways and genes associated with high-risk siALI and provide a theoretical foundation for phenotype-based molecular classification and precision therapy.

The primary function of the immune system is to detect and respond to potential threats, and distinct patterns of ICI may serve as early indicators of disease progression. Therefore, this study further investigated the IME of siALI. The results demonstrated significant differences in the infiltration levels of various immune cell subtypes between the siALI group and the sepsis-only group, including activated B cells, neutrophils, macrophages, NK T cells, eosinophils, MDSCs, and Tfh cells. In sepsis, activated B cells tend to increase over time, whereas Tfh cells exhibit a gradual decline [84]. Therefore, monitoring the proportions of these seven immune cell types may provide early warning indicators for the onset of siALI. Previous studies have shown that reduced peripheral eosinophil activity is associated with worse survival outcomes in sepsis [85]. In this study, correlation analysis among immune cells revealed a positive association between neutrophils and eosinophils, suggesting a potential synergistic role for these cell types in the transition from sepsis to siALI. By focusing on the differentially infiltrated immune cell subsets and integrating key model genes, the potential regulatory mechanisms were further examined.

S100A12 exhibited a negative correlation with activated B cells, implying a possible inhibitory effect on adaptive immune responses. The positive association between *PRTN3* and macrophages suggests a role in promoting inflammatory responses and enhancing phagocytic activity. *TLR2* was positively correlated with neutrophils, indicating its involvement in innate immune activation and NETs formation. Both *TREM1* and *SGK1* were positively correlated with Tfh cells, eosinophils, macrophages, MDSCs, NKT cells, and neutrophils, highlighting their function as immunoregulatory hubs that facilitate interactions among immune cells. *FGL2* demonstrated positive correlation with MDSCs, eosinophils, NKT cells, Tfh cells, and macrophages, suggesting its role in modulating immunosuppression and inflammatory responses during siALI progression. *TLR8* demonstrated positive correlations with eosinophils and neutrophils, and a negative correlation with activated B cells, with the strongest association observed with neutrophils ($r = 0.61$, $p < 0.05$), indicating its central role in regulating granulocyte-mediated immune responses. These findings indicate that key genes shape a unique IME by influencing the recruitment, differentiation, and functional status of immune cells, thereby driving the pathological progression of siALI. A deeper understanding of the diverse immune cell subsets and their gene-mediated interactions provides a theoretical foundation for precise disease classification and targeted interventions in siALI.

The progression of siALI is not driven by dysregulation of a single gene but rather by the coordinated activity of multiple genes. Based on the constructed mRNA-miRNA regulatory network, this study identified 35 key miRNAs potentially regulating SGK1, including miR-15a-5p, miR-16-5p, and miR-19a-3p. Suppression of miR-15a-5p maturation has been shown to reduce lipopolysaccharide-induced apoptosis in pulmonary cells [86]. miR-16-5p is considered an oncogenic miRNA. Its inhibition attenuates inflammatory responses and oxidative stress, significantly enhances pulmonary epithelial cell viability, and reduces apoptosis [87,88]. These findings highlight the essential roles of miR-15a-5p, miR-16-5p, and miR-19a-3p in regulating inflammation and immune responses, and underscore the potential of miRNAs as biomarkers of disease progression and therapeutic targets in siALI. Additionally, this study identified 46 TFs as primary regulators of the eight hub genes, forming a core transcriptional regulatory network.

Furthermore, by utilizing the CTD, our study identified 31 candidate drugs or molecular compounds targeting the model genes, including cyclosporine A, dexamethasone, estradiol, tretinoin, calcitriol, mestranol, and valproic acid. Cyclosporine A has been reported to alleviate pulmonary inflammation and improve siALI outcomes by suppressing the release of mitochondrial DNA [89]. Dexamethasone is widely used in the clinical management of ALI, and a randomized clinical trial has demonstrated its capacity to improve outcomes in patients receiving mechanical ventilation [90]. Estradiol ameliorates pulmonary edema and lung injury in a siALI mouse model by activating the PI3K/AKT/SGK1 pathway and upregulating sodium channels in alveolar epithelial cells [91]. Our study also observed decreased SGK1 expression in siALI, supporting the possibility that estradiol exerts its protective effects via this target. Additionally, other compounds such as tretinoin and calcitriol have demonstrated protective roles in ALI [92,93]. However, the mechanisms through which agents like mestranol and valproic acid modulate ALI remain poorly understood and warrant further investigation.

This study has several limitations. First, the inherent heterogeneity of siALI and the absence of detailed clinical parameters (such as age, sex, and disease severity) in some publicly available datasets prevented the incorporation of these variables into the model analysis, potentially limiting the precision and generalizability of the risk prediction model. Moreover, the external validation dataset GSE10474 differed from the training set in terms of sample source. GSE10474 was derived from plasma samples, whereas the training set primarily utilized blood or whole blood samples. Gene expression profiles may exhibit tissue-specific variability depending on the biological sample (e.g., plasma, whole blood, or blood). Future research should incorporate multicenter external validation cohorts using diverse sample types (including whole blood, plasma, and serum), alongside experimental investigations into the gene expression mechanisms across different tissue origins, to improve the clinical translational potential of the diagnostic model. Lastly, due to the limited sample size of the GEO datasets, the selection of machine learning algorithms was constrained. Validation using large-scale cohorts with detailed clinical information and the development of novel computational algorithms will be necessary to ensure the

clinical applicability and robustness of the proposed diagnostic model.

Conclusions

The study identified eight key genes (*S100A12*, *PRTN3*, *TLR2*, *TREM1*, *SGK1*, *PIK3CG*, *FGL2*, *TLR8*) associated with NETs formation, inflammation, and immune dysregulation in siALI, and developed a diagnostic model demonstrating robust predictive performance. These genes influence critical signaling pathways, including TPO, TLR, and NLR, and regulate immune cell dynamics. Additionally, several potential therapeutic agents, such as cyclosporine A and dexamethasone, were identified, offering novel insights into targeted interventions for siALI.

Availability of Data and Materials

The datasets generated and/or analyzed during the current study are available in the GEO (https://www.ncbi.nlm.nih.gov/geo/) and GeneCard (https://www.genecards.org/).

Author Contributions

All authors contributed to the study conception and design. Writing - original draft preparation: WXZ; Writing - review and editing: WXZ, XRL; Conceptualization: WXZ; Methodology: ZL; Formal analysis and investigation: JCL; Funding acquisition: XRL; Resources: ZYL; Supervision: JCP, and all authors contributed to critical revision of the manuscript for important intellectual content. All authors have participated sufficiently in the work and agreed to be accountable for all aspects of the work.

Ethics Approval and Consent to Participate

Not applicable.

Acknowledgment

Not applicable.

Funding

This work was funded by National Key R&D Program of China (No. 2023YFC3011805) and the National Natural Science Foundation of China (81960351) and the Projects of Hainan Provincial Natural Science Foundation High-level Talents (822RC835).

Conflict of Interest

The authors declare no conflict of interest.

References

[1] Evans L, Rhodes A, Alhazzani W, Antonelli M, Coopersmith CM, French C, *et al*. Surviving Sepsis Campaign: International Guidelines for Management of Sepsis and Septic Shock 2021. Critical Care Medicine. 2021; 49: e1063–e1143. https://doi.org/10.1097/CCM.0000000000005337.

[2] Bauer M, Gerlach H, Vogelmann T, Preissing F, Stiefel J, Adam D. Mortality in sepsis and septic shock in Europe, North America and Australia between 2009 and 2019- results from a systematic review and meta-analysis. Critical Care (London, England). 2020; 24: 239. https://doi.org/10.1186/s13054-020-02950-2.

[3] Sheu CC, Gong MN, Zhai R, Chen F, Bajwa EK, Clardy PF, *et al*. Clinical characteristics and outcomes of sepsis-related vs non-sepsis-related ARDS. Chest. 2010; 138: 559–567. https://doi.org/10.1378/chest.09-2933.

[4] de Grooth HJ, Tuinman PR, Girbes ARJ. The attributable mortality of acute respiratory distress syndrome. Intensive Care Medicine. 2020; 46: 1508–1509. https://doi.org/10.1007/s00134-020-06053-y.

[5] Gorman EA, O'Kane CM, McAuley DF. Acute respiratory distress syndrome in adults: diagnosis, outcomes, long-term sequelae, and management. Lancet (London, England). 2022; 400: 1157–1170. https://doi.org/10.1016/S0140-6736(22)01439-8.

[6] Beitler JR, Thompson BT, Baron RM, Bastarache JA, Denlinger LC, Esserman L, *et al*. Advancing precision medicine for acute respiratory distress syndrome. The Lancet. Respiratory Medicine. 2022; 10: 107–120. https://doi.org/10.1016/S2213-2600(21)00157-0.

[7] Zhu W, Zhang Y, Wang Y. Immunotherapy strategies and prospects for acute lung injury: Focus on immune cells and cytokines. Frontiers in Pharmacology. 2022; 13: 1103309. https://doi.org/10.3389/fphar.2022.1103309.

[8] Sun B, Lei M, Zhang J, Kang H, Liu H, Zhou F. Acute lung injury caused by sepsis: how does it happen? Frontiers in Medicine. 2023; 10: 1289194. https://doi.org/10.3389/fmed.2023.1289194.

[9] Gong T, Fu Y, Wang Q, Loughran PA, Li Y, Billiar TR, *et al*. Decoding the multiple functions of ZBP1 in the mechanism of sepsis-induced acute lung injury. Communications Biology. 2024; 7: 1361. https://doi.org/10.1038/s42003-024-07072-x.

[10] Mikacenic C, Hansen EE, Radella F, Gharib SA, Stapleton RD, Wurfel MM. Interleukin-17A Is Associated With Alveolar Inflammation and Poor Outcomes in Acute Respiratory Distress Syndrome. Critical Care Medicine. 2016; 44: 496–502. https://doi.org/10.1097/CCM.0000000000001409.

[11] Butt Y, Kurdowska A, Allen TC. Acute Lung Injury: A Clinical and Molecular Review. Archives of Pathology & Laboratory Medicine. 2016; 140: 345–350. https://doi.org/10.5858/arpa.2015-0519-RA.

[12] Poli V, Zanoni I. Neutrophil intrinsic and extrinsic regulation of NETosis in health and disease. Trends in Microbiology. 2023; 31: 280–293. https://doi.org/10.1016/j.tim.2022.10.002.

[13] Zhou X, Jin J, Lv T, Song Y. A Narrative Review: The Role of NETs in Acute Respiratory Distress Syndrome/Acute Lung Injury. International Journal of Molecular Sciences. 2024; 25: 1464. https://doi.org/10.3390/ijms25031464.

[14] Ojima M, Yamamoto N, Hirose T, Hamaguchi S, Tasaki O, Kojima T, *et al*. Serial change of neutrophil extracellular traps in tracheal aspirate of patients with acute respiratory distress syndrome: report of three cases. Journal of Intensive Care. 2020; 8: 25. https://doi.org/10.1186/s40560-020-00444-5.

[15] Zhao J, Zhen N, Zhou Q, Lou J, Cui W, Zhang G, *et al*. NETs Promote Inflammatory Injury by Activating *cGAS-STING* Pathway in Acute Lung Injury. International Journal of Molecular Sciences. 2023; 24: 5125. https://doi.org/10.3390/ijms

24065125.
[16] Auslander N, Gussow AB, Koonin EV. Incorporating Machine Learning into Established Bioinformatics Frameworks. International Journal of Molecular Sciences. 2021; 22: 2903. https://doi.org/10.3390/ijms22062903.
[17] Olivier M, Asmis R, Hawkins GA, Howard TD, Cox LA. The Need for Multi-Omics Biomarker Signatures in Precision Medicine. International Journal of Molecular Sciences. 2019; 20: 4781. https://doi.org/10.3390/ijms20194781.
[18] Wang YM, Qi X, Gong FC, Chen Y, Yang ZT, Mao EQ, *et al*. Protective and predictive role of Mucin1 in sepsis-induced ALI/ARDS. International Immunopharmacology. 2020; 83: 106438. https://doi.org/10.1016/j.intimp.2020.106438.
[19] Howrylak JA, Dolinay T, Lucht L, Wang Z, Christiani DC, Sethi JM, *et al*. Discovery of the gene signature for acute lung injury in patients with sepsis. Physiological Genomics. 2009; 37: 133–139. https://doi.org/10.1152/physiolgenomics.90275.2008.
[20] Demaret J, Venet F, Friggeri A, Cazalis MA, Plassais J, Jallades L, *et al*. Marked alterations of neutrophil functions during sepsis-induced immunosuppression. Journal of Leukocyte Biology. 2015; 98: 1081–1090. https://doi.org/10.1189/jlb.4A0415-168RR.
[21] Barrett T, Wilhite SE, Ledoux P, Evangelista C, Kim IF, Tomashevsky M, *et al*. NCBI GEO: archive for functional genomics data sets–update. Nucleic Acids Research. 2013; 41: D991–5. https://doi.org/10.1093/nar/gks1193.
[22] Davis S, Meltzer PS. GEOquery: a bridge between the Gene Expression Omnibus (GEO) and BioConductor. Bioinformatics (Oxford, England). 2007; 23: 1846–1847. https://doi.org/10.1093/bioinformatics/btm254.
[23] Kangelaris KN, Prakash A, Liu KD, Aouizerat B, Woodruff PG, Erle DJ, *et al*. Increased expression of neutrophil-related genes in patients with early sepsis-induced ARDS. American Journal of Physiology. Lung Cellular and Molecular Physiology. 2015; 308: L1102–13. https://doi.org/10.1152/ajplung.00380.2014.
[24] Dolinay T, Kim YS, Howrylak J, Hunninghake GM, An CH, Fredenburgh L, *et al*. Inflammasome-regulated cytokines are critical mediators of acute lung injury. American Journal of Respiratory and Critical Care Medicine. 2012; 185: 1225–1234. https://doi.org/10.1164/rccm.201201-0003OC.
[25] Stelzer G, Rosen N, Plaschkes I, Zimmerman S, Twik M, Fishilevich S, *et al*. The GeneCards Suite: From Gene Data Mining to Disease Genome Sequence Analyses. Current Protocols in Bioinformatics. 2016; 54: 1.30.1–1.30.33. https://doi.org/10.1002/cpbi.5.
[26] Wu J, Zhang F, Zheng X, Zhang J, Cao P, Sun Z, *et al*. Identification of renal ischemia reperfusion injury subtypes and predictive strategies for delayed graft function and graft survival based on neutrophil extracellular trap-related genes. Frontiers in Immunology. 2022; 13: 1047367. https://doi.org/10.3389/fimmu.2022.1047367.
[27] Teng ZH, Li WC, Li ZC, Wang YX, Han ZW, Zhang YP. Neutrophil extracellular traps-associated modification patterns depict the tumor microenvironment, precision immunotherapy, and prognosis of clear cell renal cell carcinoma. Frontiers in Oncology. 2022; 12: 1094248. https://doi.org/10.3389/fonc.2022.1094248.
[28] Han Y, Ding Z, Chen B, Liu Y, Liu Y. A Novel Inflammatory Response-Related Gene Signature Improves High-Risk Survival Prediction in Patients With Head and Neck Squamous Cell Carcinoma. Frontiers in Genetics. 2022; 13: 767166. https://doi.org/10.3389/fgene.2022.767166.
[29] Zhai WY, Duan FF, Chen S, Wang JY, Lin YB, Wang YZ, *et al*. A Novel Inflammatory-Related Gene Signature Based Model for Risk Stratification and Prognosis Prediction in Lung Adenocarcinoma. Frontiers in Genetics. 2022; 12: 798131. https://doi.org/10.3389/fgene.2021.798131.
[30] Chen L, Zhu G, Liu Y, Shao Y, Pan B, Zheng J. Identification of inflammatory-related gene signatures to predict prognosis of endometrial carcinoma. BMC Genomic Data. 2022; 23: 74. https://doi.org/10.1186/s12863-022-01088-0.
[31] Leek JT, Johnson WE, Parker HS, Jaffe AE, Storey JD. The sva package for removing batch effects and other unwanted variation in high-throughput experiments. Bioinformatics (Oxford, England). 2012; 28: 882–883. https://doi.org/10.1093/bioinformatics/bts034.
[32] Ben Salem K, Ben Abdelaziz A. Principal Component Analysis (PCA). La Tunisie Medicale. 2021; 99: 383–389.
[33] Ritchie ME, Phipson B, Wu D, Hu Y, Law CW, Shi W, *et al*. limma powers differential expression analyses for RNA-sequencing and microarray studies. Nucleic Acids Research. 2015; 43: e47. https://doi.org/10.1093/nar/gkv007.
[34] Zhang H, Meltzer P, Davis S. RCircos: an R package for Circos 2D track plots. BMC Bioinformatics. 2013; 14: 244. https://doi.org/10.1186/1471-2105-14-244.
[35] Robin X, Turck N, Hainard A, Tiberti N, Lisacek F, Sanchez JC, *et al*. pROC: an open-source package for R and S+ to analyze and compare ROC curves. BMC Bioinformatics. 2011; 12: 77. https://doi.org/10.1186/1471-2105-12-77.
[36] Mai HJ, Baby D, Bauer P. Black sheep, dark horses, and colorful dogs: a review on the current state of the Gene Ontology with respect to iron homeostasis in *Arabidopsis thaliana*. Frontiers in Plant Science. 2023; 14: 1204723. https://doi.org/10.3389/fpls.2023.1204723.
[37] Kanehisa M, Goto S. KEGG: kyoto encyclopedia of genes and genomes. Nucleic Acids Research. 2000; 28: 27–30. https://doi.org/10.1093/nar/28.1.27.
[38] Yu G, Wang LG, Han Y, He QY. clusterProfiler: an R package for comparing biological themes among gene clusters. Omics: a Journal of Integrative Biology. 2012; 16: 284–287. https://doi.org/10.1089/omi.2011.0118.
[39] Liu Y, Zhao H. Variable importance-weighted Random Forests. Quantitative Biology (Beijing, China). 2017; 5: 338–351.
[40] Sanz H, Valim C, Vegas E, Oller JM, Reverter F. SVM-RFE: selection and visualization of the most relevant features through non-linear kernels. BMC Bioinformatics. 2018; 19: 432. https://doi.org/10.1186/s12859-018-2451-4.
[41] Engebretsen S, Bohlin J. Statistical predictions with glmnet. Clinical Epigenetics. 2019; 11: 123. https://doi.org/10.1186/s13148-019-0730-1.
[42] Wu J, Zhang H, Li L, Hu M, Chen L, Xu B, *et al*. A nomogram for predicting overall survival in patients with low-grade endometrial stromal sarcoma: A population-based analysis. Cancer Communications (London, England). 2020; 40: 301–312. https://doi.org/10.1002/cac2.12067.
[43] Van Calster B, Wynants L, Verbeek JFM, Verbakel JY, Christodoulou E, Vickers AJ, *et al*. Reporting and Interpreting Decision Curve Analysis: A Guide for Investigators. European Urology. 2018; 74: 796–804. https://doi.org/10.1016/j.eururo.2018.08.038.
[44] Yu G, Li F, Qin Y, Bo X, Wu Y, Wang S. GOSemSim: an R package for measuring semantic similarity among GO terms and gene products. Bioinformatics (Oxford, England). 2010; 26: 976–978. https://doi.org/10.1093/bioinformatics/btq064.
[45] Subramanian A, Tamayo P, Mootha VK, Mukherjee S, Ebert BL, Gillette MA, *et al*. Gene set enrichment analysis: a knowledge-based approach for interpreting genome-wide expression profiles. Proceedings of the National Academy of Sciences of the United States of America. 2005; 102: 15545–15550. https://doi.org/10.1073/pnas.0506580102.
[46] Hao T, Peng W, Wang Q, Wang B, Sun J. Reconstruction and Application of Protein-Protein Interaction Network. International Journal of Molecular Sciences. 2016; 17: 907. https://doi.org/10.3390/ijms17060907.

[47] Szklarczyk D, Gable AL, Lyon D, Junge A, Wyder S, Huerta-Cepas J, *et al*. STRING v11: protein-protein association networks with increased coverage, supporting functional discovery in genome-wide experimental datasets. Nucleic Acids Research. 2019; 47: D607–D613. https://doi.org/10.1093/nar/gky1131.

[48] Mostafavi S, Morris Q. Combining many interaction networks to predict gene function and analyze gene lists. Proteomics. 2012; 12: 1687–1696. https://doi.org/10.1002/pmic.201100607.

[49] Zhou KR, Liu S, Sun WJ, Zheng LL, Zhou H, Yang JH, *et al*. ChIPBase v2.0: decoding transcriptional regulatory networks of non-coding RNAs and protein-coding genes from ChIP-seq data. Nucleic Acids Research. 2017; 45: D43–D50. https://doi.org/10.1093/nar/gkw965.

[50] Li JH, Liu S, Zhou H, Qu LH, Yang JH. starBase v2.0: decoding miRNA-ceRNA, miRNA-ncRNA and protein-RNA interaction networks from large-scale CLIP-Seq data. Nucleic Acids Research. 2014; 42: D92–7. https://doi.org/10.1093/nar/gkt1248.

[51] Grondin CJ, Davis AP, Wiegers JA, Wiegers TC, Sciaky D, Johnson RJ, *et al*. Predicting molecular mechanisms, pathways, and health outcomes induced by Juul e-cigarette aerosol chemicals using the Comparative Toxicogenomics Database. Current Research in Toxicology. 2021; 2: 272–281. https://doi.org/10.1016/j.crtox.2021.08.001.

[52] Shannon P, Markiel A, Ozier O, Baliga NS, Wang JT, Ramage D, *et al*. Cytoscape: a software environment for integrated models of biomolecular interaction networks. Genome Research. 2003; 13: 2498–2504. https://doi.org/10.1101/gr.1239303.

[53] Xiao B, Liu L, Li A, Xiang C, Wang P, Li H, *et al*. Identification and Verification of Immune-Related Gene Prognostic Signature Based on ssGSEA for Osteosarcoma. Frontiers in Oncology. 2020; 10: 607622. https://doi.org/10.3389/fonc.2020.607622.

[54] Reis e Sousa C, Yamasaki S, Brown GD. Myeloid C-type lectin receptors in innate immune recognition. Immunity. 2024; 57: 700–717. https://doi.org/10.1016/j.immuni.2024.03.005.

[55] Price DR, Garcia JGN. A Razor's Edge: Vascular Responses to Acute Inflammatory Lung Injury/Acute Respiratory Distress Syndrome. Annual Review of Physiology. 2024; 86: 505–529. https://doi.org/10.1146/annurev-physiol-042222-030731.

[56] Sung PS, Peng YC, Yang SP, Chiu CH, Hsieh SL. CLEC5A is critical in Pseudomonas aeruginosa-induced NET formation and acute lung injury. JCI Insight. 2022; 7: e156613. https://doi.org/10.1172/jci.insight.156613.

[57] Duan T, Du Y, Xing C, Wang HY, Wang RF. Toll-Like Receptor Signaling and Its Role in Cell-Mediated Immunity. Frontiers in Immunology. 2022; 13: 812774. https://doi.org/10.3389/fimmu.2022.812774.

[58] Anwar HM, Salem GEM, Abd El-Latief HM, Osman AAE, Ghanem SK, Khan H, *et al*. Therapeutic potential of proteases in acute lung injury and respiratory distress syndrome via TLR4/Nrf2/NF-kB signaling modulation. International Journal of Biological Macromolecules. 2024; 267: 131153. https://doi.org/10.1016/j.ijbiomac.2024.131153.

[59] Xia P, Ji X, Yan L, Lian S, Chen Z, Luo Y. Roles of S100A8, S100A9 and S100A12 in infection, inflammation and immunity. Immunology. 2024; 171: 365–376. https://doi.org/10.1111/imm.13722.

[60] Zhang Z, Han N, Shen Y. S100A12 promotes inflammation and cell apoptosis in sepsis-induced ARDS via activation of NLRP3 inflammasome signaling. Molecular Immunology. 2020; 122: 38–48. https://doi.org/10.1016/j.molimm.2020.03.022.

[61] Camoretti-Mercado B, Karrar E, Nuñez L, Bowman MAH. S100A12 and the Airway Smooth Muscle: Beyond Inflammation and Constriction. Journal of Allergy & Therapy. 2012; 3: S1–007. https://doi.org/10.4172/2155-6121.S1-007.

[62] Kikkawa T, Sato N, Kojika M, Takahashi G, Aoki K, Hoshikawa K, *et al*. Significance of measuring S100A12 and sRAGE in the serum of sepsis patients with postoperative acute lung injury. Digestive Surgery. 2010; 27: 307–312. https://doi.org/10.1159/000313687.

[63] Jiang J, Chen H, Zhao C, Li T, Zhang C, Ma L, *et al*. PRTN3 promotes IL33/Treg-mediated tumor immunosuppression by enhancing the M2 polarization of tumor-associated macrophages in lung adenocarcinoma. Cancer Letters. 2025; 616: 217584. https://doi.org/10.1016/j.canlet.2025.217584.

[64] Saheb Sharif-Askari N, Saheb Sharif-Askari F, Ahmed SBM, Hannawi S, Hamoudi R, Hamid Q, *et al*. Enhanced Expression of Autoantigens During SARS-CoV-2 Viral Infection. Frontiers in Immunology. 2021; 12: 686462. https://doi.org/10.3389/fimmu.2021.686462.

[65] Simpson ME, Petri WA, Jr. TLR2 as a Therapeutic Target in Bacterial Infection. Trends in Molecular Medicine. 2020; 26: 715–717. https://doi.org/10.1016/j.molmed.2020.05.006.

[66] Yao M, Fang C, Wang Z, Guo T, Wu D, Ma J, *et al*. miR-328-3p targets TLR2 to ameliorate oxygen-glucose deprivation injury and neutrophil extracellular trap formation in HUVECs via inhibition of the NF-κB signaling pathway. PloS One. 2024; 19: e0299382. https://doi.org/10.1371/journal.pone.0299382.

[67] Strong EJ, Wang J, Ng TW, Porcelli SA, Lee S. Mycobacterium tuberculosis PPE51 Inhibits Autophagy by Suppressing Toll-Like Receptor 2-Dependent Signaling. mBio. 2022; 13: e0297421. https://doi.org/10.1128/mbio.02974-21.

[68] Park SY, Shrestha S, Youn YJ, Kim JK, Kim SY, Kim HJ, *et al*. Autophagy Primes Neutrophils for Neutrophil Extracellular Trap Formation during Sepsis. American Journal of Respiratory and Critical Care Medicine. 2017; 196: 577–589. https://doi.org/10.1164/rccm.201603-0596OC.

[69] Xu X, Zhi T, Chao H, Jiang K, Liu Y, Bao Z, *et al*. ERK1/2/mTOR/Stat3 pathway-mediated autophagy alleviates traumatic brain injury-induced acute lung injury. Biochimica et Biophysica Acta. Molecular Basis of Disease. 2018; 1864: 1663–1674. https://doi.org/10.1016/j.bbadis.2018.02.011.

[70] Li C, Cai C, Xu D, Chen X, Song J. TREM1: Activation, signaling, cancer and therapy. Pharmacological Research. 2024; 204: 107212. https://doi.org/10.1016/j.phrs.2024.107212.

[71] Oudhuis GJ, Beuving J, Bergmans D, Stobberingh EE, ten Velde G, Linssen CF, *et al*. Soluble Triggering Receptor Expressed on Myeloid cells-1 in bronchoalveolar lavage fluid is not predictive for ventilator-associated pneumonia. Intensive Care Medicine. 2009; 35: 1265–1270. https://doi.org/10.1007/s00134-009-1463-y.

[72] Ventetuolo CE, Levy MM. Biomarkers: diagnosis and risk assessment in sepsis. Clinics in Chest Medicine. 2008; 29: 591–603, vii. https://doi.org/10.1016/j.ccm.2008.07.001.

[73] Tammaro A, Scantlebery AML, Rampanelli E, Borrelli C, Claessen N, Butter LM, *et al*. TREM1/3 Deficiency Impairs Tissue Repair After Acute Kidney Injury and Mitochondrial Metabolic Flexibility in Tubular Epithelial Cells. Frontiers in Immunology. 2019; 10: 1469. https://doi.org/10.3389/fimmu.2019.01469.

[74] Bian X, Xue H, Jing D, Wang Y, Zhou G, Zhu F. Role of Serum/Glucocorticoid-Regulated Kinase 1 (SGK1) in Immune and Inflammatory Diseases. Inflammation. 2023; 46: 1612–1625. https://doi.org/10.1007/s10753-023-01857-8.

[75] Li J, Liu L, Zhou X, Lu X, Liu X, Li G, *et al*. Melatonin Attenuates Sepsis-Induced Acute Lung Injury Through Improvement of Epithelial Sodium Channel-Mediated Alveolar Fluid Clearance Via Activation of SIRT1/SGK1/Nedd4-2 Signaling Pathway. Frontiers in Pharmacology. 2020; 11: 590652. https://doi.org/10.3389/fphar.2020.590652.

[76] Wang C, Sun H, Wang R, Ma X, Sun Y. FGL2: A new target molecule for coagulation and immune regulation in infectious disease. International Immunopharmacology. 2024; 143: 113505. https://doi.org/10.1016/j.intimp.2024.113505.

[77] Sun R, Ding J, Yang Y, Wu F, Wang X, Liu M, *et al*. Trichinella

spiralis alleviates LPS-induced acute lung injury by modulating the protective Th2 immune response. Veterinary Parasitology. 2025; 333: 110206. https://doi.org/10.1016/j.vetpar.2024.110206.

[78] Lei J, Zhou Y, Zhao H, Chen Y, Yan G, Wu L, *et al*. Dabigatran activates inflammation resolution by promoting fibrinogen-like protein 2 shedding and $RvD5_{n\text{-}3\ DPA}$ production. Theranostics. 2021; 11: 4251–4261. https://doi.org/10.7150/thno.50182.

[79] Zhou Y, Lei J, Xie Q, Wu L, Jin S, Guo B, *et al*. Fibrinogen-like protein 2 controls sepsis catabasis by interacting with resolvin Dp5. Science Advances. 2019; 5: eaax0629. https://doi.org/10.1126/sciadv.aax0629.

[80] Martínez-Espinoza I, Guerrero-Plata A. The Relevance of TLR8 in Viral Infections. Pathogens (Basel, Switzerland). 2022; 11: 134. https://doi.org/10.3390/pathogens11020134.

[81] Bendelja K, Vojvoda V, Aberle N, Cepin-Bogovic J, Gagro A, Mlinaric-Galinovic G, *et al*. Decreased Toll-like receptor 8 expression and lower TNF-α synthesis in infants with acute RSV infection. Respiratory Research. 2010; 11: 143. https://doi.org/10.1186/1465-9921-11-143.

[82] Lee N, Ko R, Lee SY. Differential Expression Patterns of Toll-like Receptors in COVID-19 Patients. Frontiers in Bioscience (Landmark Edition). 2023; 28: 307. https://doi.org/10.31083/j.fbl2811307.

[83] Maus UA, Backi M, Winter C, Srivastava M, Schwarz MK, Rückle T, *et al*. Importance of phosphoinositide 3-kinase gamma in the host defense against pneumococcal infection. American Journal of Respiratory and Critical Care Medicine. 2007; 175: 958–966. https://doi.org/10.1164/rccm.200610-1533OC.

[84] Huang L, Wu C, Xu D, Cui Y, Tang J. Screening of Important Factors in the Early Sepsis Stage Based on the Evaluation of ssGSEA Algorithm and ceRNA Regulatory Network. Evolutionary Bioinformatics Online. 2021; 17: 11769343211058463. https://doi.org/10.1177/11769343211058463.

[85] Al Duhailib Z, Farooqi M, Piticaru J, Alhazzani W, Nair P. The role of eosinophils in sepsis and acute respiratory distress syndrome: a scoping review. Canadian Journal of Anaesthesia = Journal Canadien D'anesthesie. 2021; 68: 715–726. https://doi.org/10.1007/s12630-021-01920-8.

[86] Hong X, Li S, Wang J, Zhao Z, Feng Z. Circular RNA circFADS2 is overexpressed in sepsis and suppresses LPS-induced lung cell apoptosis by inhibiting the maturation of miR-15a-5p. BMC Immunology. 2021; 22: 29. https://doi.org/10.1186/s12865-021-00419-7.

[87] Ghafouri-Fard S, Khoshbakht T, Hussen BM, Abdullah ST, Taheri M, Samadian M. A review on the role of mir-16-5p in the carcinogenesis. Cancer Cell International. 2022; 22: 342. https://doi.org/10.1186/s12935-022-02754-0.

[88] Song X, Li L, Zhao Y, Song Y. Down-regulation of long non-coding RNA XIST aggravates sepsis-induced lung injury by regulating miR-16-5p. Human Cell. 2021; 34: 1335–1345. https://doi.org/10.1007/s13577-021-00542-y.

[89] Xiao Z, Jia B, Zhao X, Bi S, Meng W. Attenuation of Lipopolysaccharide-Induced Acute Lung Injury by Cyclosporine-A via Suppression of Mitochondrial DNA. Medical Science Monitor: International Medical Journal of Experimental and Clinical Research. 2018; 24: 7682–7688. https://doi.org/10.12659/MSM.909909.

[90] Maveddat A, Mallah H, Rao S, Ali K, Sherali S, Nugent K. Severe Acute Respiratory Distress Syndrome Secondary to Coronavirus 2 (SARS-CoV-2). The International Journal of Occupational and Environmental Medicine. 2020; 11: 157–178. https://doi.org/10.34172/ijoem.2020.2202.

[91] Qi D, He J, Wang D, Deng W, Zhao Y, Ye Y, *et al*. 17β-estradiol suppresses lipopolysaccharide-induced acute lung injury through PI3K/Akt/SGK1 mediated up-regulation of epithelial sodium channel (ENaC) in vivo and in vitro. Respiratory Research. 2014; 15: 159. https://doi.org/10.1186/s12931-014-0159-1.

[92] Li S, Lei Y, Lei J, Li H. All trans retinoic acid promotes macrophage phagocytosis and decreases inflammation via inhibiting CD14/TLR4 in acute lung injury. Molecular Medicine Reports. 2021; 24: 868. https://doi.org/10.3892/mmr.2021.12508.

[93] Yeh CL, Wu JM, Su LH, Yang PJ, Lee PC, Chen KY, *et al*. Intravenous calcitriol administration regulates the renin-angiotensin system and attenuates acute lung injury in obese mice complicated with polymicrobial sepsis. Biomedicine & Pharmacotherapy = Biomedecine & Pharmacotherapie. 2021; 141: 111856. https://doi.org/10.1016/j.biopha.2021.111856.